M 2023

U.PORTO
FEUP FACULDADE DE ENGENHARIA
UNIVERSIDADE DO PORTO

# METHANATION OF $CO_2$ IN A SORPTION-ENHANCED REACTOR

**VASCO FILIPE MOREIRA RIBEIRO**

MASTER THESIS IN CHEMICAL ENGINEERING
PRESENTED TO THE FACULTY OF ENGINEERING
OF THE UNIVERSITY OF PORTO

Master in Chemical Engineering

# *Methanation of $CO_2$ in a Sorption-Enhanced Reactor*

## Master dissertation

of

**Vasco Filipe Moreira Ribeiro**

**Developed within the course of dissertation**

held in

**LEPABE – Laboratory for Process Engineering, Environment, Biotechnology and Energy**




Supervisor at FEUP: **Prof. Luís Miguel Madeira**

Joint supervisor at FEUP: **Doctor Miguel Angel Soria**







**July 2023**

# Acknowledgments

Firstly, I would like to thank my supervisors, Professor Luís Miguel Madeira and Doctor Miguel Angel Soria, for all the guidance and support provided during the development of the dissertation.

Also, to all the LEPABE colleagues, for always being ready to help and for keeping a relaxed atmosphere in the lab, and to Cristina Caeiro, for providing me with her results and being ready to answer my doubts.

To my lifelong friends, a special thanks, and may we never lack plans scheduled at the last minute.

I want to say thank you to all my ballet girls, in special, to Kika and Mariana, for sharing the most magical moments on stage with me and being my biggest supporters (and, of course, for always reminding me I am the favorite one).

To my unique group of friends, my Qmugas para Semore. There are hardly enough words to describe how important you were during these 5 years. Thank you for being the party buddies and the study mates, for cheering me up and always showing your support, but most importantly, for being so special and having such an impact on me.

To the best gift Oulu could have given me and to my soulmate, Matilde. Thank you for always being one call away and for being so close, although far sometimes. Thank you for being a safe place and the best listener. This last year would not mean the same if it was not for you.

Finally, the greatest thanks go to my family, especially my parents, siblings and my grandmother. Thank you for always being there for me and for being able to handle my most complicated stressful mood. Most importantly, thank you for always supporting and encouraging my decisions and for never letting me give up.

This work was financially supported by LA/P/0045/2020 (ALiCE), UIDB/00511/2020 and UIDP/00511/2020 (LEPABE), funded by national funds through FCT/MCTES (PIDDAC).

fct Fundação para a Ciência e a Tecnologia

REPÚBLICA PORTUGUESA

# Abstract

Climate change represents one of today's major concerns, being mainly caused by the increase of greenhouse gases emissions, especially carbon dioxide, as a result of the industrialization era. Hence, considering the continuous population growth and, consequently, the increasing energy demand, it is of high importance to develop new strategies to combat this issue. The concept of Power-to-Methane arises as a technology that consists of using $CO_2$, e.g. captured from the burning of fossil fuels, and $H_2$, from electrolysis of water, to produce renewable methane (through the Sabatier reaction), able to substitute natural gas. The Sabatier (or methanation) reaction can also be directly applied to a stream of biogas, in order to upgrade its content on $CH_4$ and, therefore, widen its applications. However, the existing methane present in biogas limits the $CO_2$ conversion in such reversible reaction. Thus, the present work aims to study a sorption-enhanced reactor (SER) on the enhancement of the $CO_2$ methanation process, by removing one of the reaction by-products, water, using a selective adsorbent and, consequently, shifting the reaction equilibrium.

At first, three different catalysts were screened and the best option (a Ni-based catalyst) was chosen to perform several tests to analyse the influence of various parameters (reaction temperature, catalyst reduction temperature, gas velocity, total pressure and feed composition) in process performance. It was found that $CO_2$ conversion increased for higher temperatures and pressures, while the increase in the catalyst reduction temperature (from 650 to 800 °C) produced negative effects on the performance. Variations in gas velocity and feed composition (by withdrawing $N_2$ from the feed) produced no significant differences in carbon dioxide conversion.

The influence of pressure on water adsorption was assessed using zeolite 13X, a promising adsorbent that was selected based on previous works. Hence, it was proved that higher adsorption capacities are obtained for higher pressures.

Finally, the SER performance was assessed using the best option from the catalysts and zeolite 13X, allowing the obtention of 100 % $CO_2$ conversion for a period of time (i.e., before the water breakthrough) and proving the advantages of using the adsorptive reactor on the methanation process as compared to a traditional packed-bed reactor. Additionally, it was shown that increasing pressure led to an increase in the breakthrough time, consequently increasing the period of time while $CO_2$ conversion was complete.

**Keywords:** Power-to-Methane; Methanation catalyst; Water adsorbent; Sorption-enhanced reactor

# Resumo

As alterações climáticas representam uma das maiores preocupações da atualidade, sendo causadas principalmente pelo aumento das emissões de gases com efeito de estufa, em especial dióxido de carbono, como resultado da era da industrialização. Assim, tendo em conta o contínuo crescimento populacional e, consequentemente, o aumento da necessidade energética, é de elevada importância o desenvolvimento de novas estratégias para combater este problema. O conceito de Potência elétrica-para-Metano surge como uma tecnologia que consiste na utilização de $CO_2$, por exemplo, capturado da queima de combustíveis fósseis, e $H_2$, proveniente da eletrólise da água, para produzir metano renovável (através da reação de *Sabatier)*, capaz de substituir o gás natural. A reação de *Sabatier* (ou de metanação) pode também ser aplicada diretamente a uma corrente de biogás, a fim de aumentar o seu teor em $CH_4$ e, por conseguinte, alargar as suas aplicações. No entanto, o metano presente no biogás limita a conversão do $CO_2$ nesta reação reversível. Assim, o presente trabalho tem como objetivo estudar um reator adsortivo (SER – sorption-enhanced reactor) na melhoria do processo de metanação do $CO_2$, através da remoção de um dos produtos secundários da reação, a água, utilizando um adsorvente seletivo e, consequentemente, deslocando o equilíbrio da reação.

Numa primeira fase, foram selecionados três catalisadores diferentes e a melhor opção (um catalisador à base de Níquel) foi escolhido para se realizarem vários testes para analisar-se a influência de vários parâmetros (temperatura de reação, temperatura de redução do catalisador, velocidade do gás, pressão total e composição da alimentação) no desempenho do processo. Verificou-se que a conversão de $CO_2$ aumentava para temperaturas e pressões mais elevadas, enquanto o aumento da temperatura de redução do catalisador (de 650 para 800 °C) produzia efeitos negativos no desempenho. As variações na velocidade do gás e na composição da alimentação (retirando $N_2$ da alimentação) não produziram diferenças significativas na conversão de dióxido de carbono.

A influência da pressão na adsorção de água foi avaliada utilizando o zeólito 13X, um adsorvente promissor escolhido com base em trabalhos anteriores. Assim, provou-se que se obtêm maiores capacidades de adsorção com pressões mais elevadas.

Finalmente, o desempenho do SER foi avaliado utilizando a melhor opção dos catalisadores e o zeólito 13X, permitindo a obtenção de 100 % de conversão de $CO_2$ durante um período (i.e., antes do *rutura* da água) e provando as vantagens da utilização do reator adsortivo no processo de metanação comparativamente a um reator tradicional de leito fixo. Além disso, observou-se que a pressão aumenta o tempo de *rutura*, aumentando o tempo durante o qual a conversão é total.

**Palavras-chave:** *Potência elétrica-para-Metano*; Catalisador de metanação; Adsorvente de água; Reator adsortivo

# Declaration

I hereby declare, under word of honour, that this work is original and that all non-original contributions are indicated and due reference is given to the author and source.

Vasco Filipe Moreira Ribeiro

*Porto, 3 July 2023*

# Index

**1 Introduction ..... 1**

**1.1 Framing and presentation of the work ..... 1**

**1.2 Contribution of the author to the work ..... 3**

**1.3 Organization of the dissertation ..... 3**

**2 Context and State of the art ..... 5**

**2.1 Methanation Catalysts ..... 5**

**2.2 Water Adsorbents ..... 7**

**2.3 Sorption-Enhanced Reactor ..... 10**

**3 Materials and Methods ..... 15**

**3.1 Catalytic tests ..... 15**

**3.2 Adsorption tests ..... 18**

**3.3 SER tests ..... 19**

**4 Results and discussion ..... 23**

**4.1 Catalytic tests ..... 23**

4.1.1 Catalytic screening and effect of reaction temperature ..... 23

4.1.2 Effect of reduction temperature ..... 24

4.1.3 Effect of gas velocity ..... 24

4.1.4 Effect of total pressure ..... 25

4.1.5 Effect of feed composition ..... 26

**4.2 Adsorption tests ..... 27**

**4.3 SER tests ..... 30**

**5 Conclusions ..... 37**

**6 Assessment of the work done ..... 39**

**6.1 Objectives Achieved ..... 39**

**6.2 Final Assessment ..... 39**

**7 References ..... 41**

# List of Figures

*Figure 1.1. Annual $CO_2$ emissions from fossil fuels worldwide, adapted from [4]. ..... 1*

*Figure 2.1. Temperature and pressure influence on $CO_2$ conversion (for $H_2/CO_2 = 4$), extracted from [13]. ..... 5*

*Figure 2.2. Examples of breakthrough curves: (a) - poorly adsorbed; (b) – commonly cases, (c) – strongly adsorbed with no mass-transfer effect, extracted from [40]. ..... 8*

*Figure 2.3. Adsorption breakthrough curves of water on 3A zeolite at different temperatures, extracted from [50]. ..... 10*

*Figure 2.4. Schematic representation of a traditional reactor (on the left) and a SER (on the right).. 11*

*Figure 2.5. $CO_2$ conversion achieved after adsorbent saturation for 5Ni/5A (blue) and 5Ni/13X (black) at 300 ºC, extracted from [45]..... 12*

*Figure 2.6. Normalized time of operation (NTO) as a function of the number of cycles, adapted from [45]. ..... 13*

*Figure 3.1. Scheme of the experimental setup for the catalytic tests, adapted from [60]. ..... 15*

*Figure 3.2. TPR-$H_2$ results for two catalysts: 0.5 % $Ru/Al_2O_3$ (on the left) and for $NiO/Al_2O_3$-$SiO_2$-CeO (on the right). ..... 17*

*Figure 3.3. Scheme of the experimental setup for the adsorption tests. ..... 18*

*Figure 3.4. Scheme of the experimental setup for the SER tests, adapted from [60]. ..... 20*

*Figure 4.1. Effect of temperature in $CO_2$ conversion for P = 1 bar, $WHSV_{CO2} = 3\ Ln \cdot g^{-1} \cdot h^{-1}$ and $H_2/CO_2$ molar ratio = 4. The bars in lighter colours represent the selectivity to methane obtained for each experiment. The dashed line represents the thermodynamic equilibrium. ..... 23*

*Figure 4.2. Effect of reduction temperature on $CO_2$ conversion at different temperatures for P = 1 bar, $WHSV_{CO2} = 3\ Ln \cdot g^{-1} \cdot h^{-1}$ and $H_2/CO_2$ molar ratio = 4. The dashed line represents the thermodynamic equilibrium. ..... 24*

*Figure 4.3. Effect of the gas velocity on $CO_2$ conversion at different temperatures for P = 1 bar, $WHSV_{CO2} = 3\ Ln \cdot g^{-1} \cdot h^{-1}$ and $H_2/CO_2$ molar ratio = 4. The dashed lines represent the average $X_{CO2}$ obtained for each temperature..... 25*

*Figure 4.4. Effect of pressure on $CO_2$ conversion at different temperatures for $WHSV_{CO2} = 3\ Ln \cdot g^{-1} \cdot h^{-1}$ and $H_2/CO_2$ molar ratio = 4. The dashed lines represent the thermodynamic equilibrium for each pressure. ..... 25*

*Figure 4.5. Effect of feed composition on $CO_2$ conversion at different temperatures for P = 1 bar, $WHSV_{CO2} = 3\ Ln \cdot g^{-1} \cdot h^{-1}$ and $H_2/CO_2$ molar ratio = 4. The dashed line represents the thermodynamic equilibrium. The striped bars represent the temperature increment in the reactor bed at steady state. ..... 26*

*Figure 4.6. Example of an $H_2O$ breakthrough curve, obtained at 250 ºC and 4 bar, until de saturation point (i.e., $y_{H2O,out}/y_{H2O,in}=1$).* ..... 28

*Figure 4.7. Adsorption of $H_2O$ over zeolite 13X through experimental data (dots) and Langmuir-Freundlich predicted model (line), at 250 ºC.* ..... 30

*Figure 4.8. SER performance at 250 ºC and 1 (A), 4 (B) and 6 (C) bar for $WHSV_{CO2}$ = 3 $Ln \cdot g^{-1} \cdot h^{-1}$ and $H_2/CO_2$ molar ratio = 4. The dotted black line represents the thermodynamic equilibrium calculated for the traditional reactor.* ..... 31

*Figure 4.9. Temperature profiles obtained inside the reactor/column for the catalytic ($T_1$ and $T_2$) and adsorption ($T_3$ and $T_4$) tests, respectively, at 250 ºC and 4 bar.* ..... 32

*Figure 4.10. $CO_2$ breakthrough curve for a feed composition of 7 $mLn \cdot min^{-1}$ of $CO_2$ and 93 $mLn \cdot min^{-1}$ of $N_2$, at 250 ºC and 4 bar.* ..... 34

*Figure 4.11. $CO_2$ flow rate at the outlet for a feed composition of 10 $mLn \cdot min^{-1}$ of $CO_2$, 40 $mLn \cdot min^{-1}$ of $H_2$ and 50 $mLn \cdot min^{-1}$ of $N_2$, at 250 ºC and 4 bar.* ..... 35

*Figure 4.12. Schematic representation of a process running in two sorption-enhanced-reactors.* ..... 36

# List of Tables

*Table 3.1. Reduction temperature used for each catalyst. ..... 17*

*Table 3.2. Operating conditions used in the experimental tests, for $WHSV_{CO2}$ = 3 $Ln \cdot g^{-1} \cdot h^{-1}$..... 18*

*Table 4.1. Experimental results obtained for the adsorption experiments, at 250 ºC..... 29*

*Table 4.2. Fitted Langmuir-Freundlich parameters for water adsorption on zeolite 13X. ..... 30*

*Table 4.3. $CO_2$ conversion obtained, at steady state, for the SER and the TR..... 33*

# Notation and Glossary

| | | |
|---|---|---|
| $F$ | molar flow rate | $mol \cdot min^{-1}$ |
| $K_{LF}$ | Langmuir-Freundlich adsorption constant | $bar^{-1}$ |
| $m$ | mass | g |
| $n$ | dimensionless empirical constant | |
| $p$ | partial pressure | bar |
| $P$ | total pressure | bar |
| $q$ | adsorption capacity | $mol \cdot g^{-1}$ |
| $Q$ | flow rate | $mLn \cdot min^{-1}$ |
| $q_{max}$ | maximum adsorption capacity | $mol \cdot g^{-1}$ |
| $S$ | selectivity | |
| $T$ | temperature | °C |
| $t$ | time | s |
| $X$ | conversion | |
| $y$ | molar fraction | |
| $\Delta H$ | enthalpy variation | $kJ \cdot mol^{-1}$ |
| $\Delta T$ | temperature variation | °C |

### *Indexes*

| | |
|---|---|
| ads | related to adsorbent |
| cat | related to catalyst |
| eq | related to equilibrium conditions |
| LF | related to Langmuir-Freundlich |
| $i$ | related to species $i$ |
| in | related to reactor inlet |
| out | related to reactor outlet |
| s | related to saturation conditions |

### *List of Acronyms*

| | |
|---|---|
| CCS | Carbon Capture and Storage |
| FID | Flame Ionization Detector |
| GHG | Greenhouse Gases |
| MOF | Metal-Organic Framework |
| NTO | Normalized Time of Operation |
| PtG | Power-to-Gas |
| PtM | Power-to-Methane |
| PSA | Pressure Swing Adsorption |
| RWGS | Reverse-Water Gas Shift |
| SER | Sorption-Enhanced Reactor |
| SiC | Silicon Carbide |
| SNG | Synthetic Natural Gas |
| TC | Temperature Controller |
| TCD | Thermal Conductivity Detector |
| TPR | Temperature Programmed Reduction |
| TSA | Thermal Swing Adsorption |
| TR | Traditional Reactor |
| VOC | Volatile Organic Compound |
| WHSV | Weight Hourly Space Velocity |

# 1 Introduction

## 1.1 Framing and presentation of the work

The natural levels of greenhouse gases (GHGs) in the atmosphere play a crucial role in supporting life on earth. However, due to the industrialization era, GHG emissions have increased and caused what is commonly known as the greenhouse effect. This effect is one of the main causes of climate change [1].

In order to achieve the 2030 Agenda for Sustainable Development, it is imperative to take actions to combat climate change. Besides that, the Paris Agreement aims to limit global warming to 1.5 ºC above pre-industrial levels, which can only be achieved by drastically reducing GHG emissions [2].

Carbon dioxide is one of the most problematic GHG due to the amounts released to the atmosphere. Before the Industrial Revolution its' emissions were very low and resulted mainly from the burning of biomass fuels. However, from the mid-20$^{th}$ century on, with global industrialization and population growth came an increased demand for energy, requiring the massive use of fossil fuels and, consequently, an increase in $CO_2$ emissions [3]. Figure 1.1 shows the increase in annual $CO_2$ emissions from fossil fuels worldwide.




*Figure 1.1. Annual $CO_2$ emissions from fossil fuels worldwide, adapted from [4].*

Some authors state that fossil fuels will still account for over 65 % of the energy mix by 2100, making the investment in technologies related to carbon dioxide capture and utilization fundamental [5].

There are already several technologies that aim to use the produced by the burning of fossil fuels, for example its capture and sequestration in suitable geological formations (Carbon

Capture and Storage – CCS). Although CCS is not yet a complete long-term solution, it is considered to be a crucial element in achieving a circular economy, as the captured $CO_2$ can be subsequently used in the production of chemicals and fuels (Carbon Capture and Use - CCU), using solar and wind technologies [6].

Taking this into account, the Power-to-Gas (PtG) concept arises with the goal of avoiding the waste of renewable energy in off-peak periods by using it to produce gaseous fuels [7]. More specifically, Power-to-Methane (PtM) consists of the production of renewable methane by using $H_2$ from electrolysis of water, that uses renewable energy, and the captured $CO_2$, producing the so called synthetic natural gas (SNG) through the exothermic Sabatier reaction (Eq. 1.1) [8, 9].

$$CO_2 + 4H_2 \rightleftharpoons CH_4 + 2H_2O \qquad \Delta H_{(298\,K)} = -165\ kJ \cdot mol^{-1} \qquad (1.1)$$

Along with the Sabatier (also known as methanation) reaction, there is the possibility that the reverse-water gas shift (RWGS) reaction might also occur (Eq. 1.2). Nevertheless, most of the commonly used methanation catalysts present very low selectivity towards CO, especially if the reaction occurs at low temperatures.

$$CO_2 + H_2 \rightleftharpoons CO + H_2O \qquad \Delta H_{(298\,K)} = 41\ kJ \cdot mol^{-1} \qquad (1.2)$$

Considering the production and storage in the framework of PtG technologies, methane can be considered a better option than hydrogen as it is a hydrogen-rich energy carrier with high energy density. Besides that, when it comes to synthesizing chemical energy carriers that can be introduced into the (already existing) natural gas infrastructure, methane is the optimal choice [8, 9].

Taking this into account and considering the urgent need to reduce the use of fossil fuels, namely natural gas, interest and developments in producing renewable alternatives have been increasing, particularly biogas [10]. Biogas is formed through anaerobic digestion, a biological process that converts organic substrates into $CH_4$ (50-70 %), $CO_2$ (30-50 %) and other minor components like hydrogen sulfide, oxygen, nitrogen or volatile organic compounds (VOC's) [10, 11].

Some of the applications of biogas include heating and electricity generation. Nevertheless, the application areas can be widened if the content in $CH_4$ in biogas is upgraded to at least 95 %, allowing the direct injection in the natural gas grid and its use as vehicle fuel [11]. The process of biogas upgrade can be achieved by simple separation of its constituents or, alternatively, by converting the $CO_2$ present in biogas into methane. Hence, applying the Sabatier reaction to a biogas stream appears as a promising solution to produce a methane-rich stream, usually called biomethane [11]. However, the existing methane in biogas limits the $CO_2$ conversion of the reversible methanation reaction making it necessary to develop technologies to overcome this issue.

One option is to remove water, a reaction by-product, from the reaction zone using a selective adsorbent, thereby shifting the methanation reaction forward in an innovative sorption-enhanced reactor (SER), and thus overcoming thermodynamic restrictions and improving the global process efficiency.

This work aims to study a SER on the enhancement of the $CO_2$ methanation process, namely by studying its impact on $CO_2$ conversion, with the objective of understanding the advantages of its use. Besides that, catalysts are to be tested and screened using a traditional reactor, based on their $CO_2$ conversion, in order to choose the best candidate to be incorporated on the SER. Finally, an adsorbent is to be tested and characterized based on its $H_2O$ adsorption capacity and cyclic stability.

## 1.2 Contribution of the author to the work

The main objective of this work was to study a sorption-enhanced reactor on $CO_2$ methanation and evaluate the advantages of its use, namely by comparing its performance with a traditional (packed-bed) reactor. Hence, the work developed can be divided into three parts, as described below.

i) The catalytic tests, in which three catalysts were tested and compared based on $CO_2$ conversion and the best candidate was used to perform a parametric study.

ii) The adsorption tests, in which the variation of adsorption capacity with pressure was studied for zeolite 13X (selected based on previous work carried out at the group).

iii) The SER tests, in which the proof-of-concept and the performance of the SER was evaluated, as well as its dependency over pressure.

All the tests mentioned above were performed by the author. However, the TPR results used to justify the reduction temperatures for each catalyst were obtained and provided by Cristina Caeiro. Also, the water-selective adsorbent choice was based on results obtained by Cristina Caeiro.

## 1.3 Organization of the dissertation

The present work is divided into 6 main chapters.

Chapter 1 presents the framework of the work, warning about climate change and pointing to the need of reducing the use of fossil fuels and increase the use of renewable sources, such as methane. Thus, the concept of Power-to-Methane is introduced, as well as an innovative technology to improve its efficiency – the sorption-enhanced reactor.

Chapter 2 presents the $CO_2$ methanation reaction and water adsorption state-of-water, namely by introducing and comparing the most commonly used catalysts and adsorbents and presenting the conclusions of several studies. Finally, the sorption-enhanced reactor is addressed, as well as some of its characteristics, and some previous studies are reviewed.

Chapter 3 describes the materials, experimental setups and procedures used to perform the tests for this work: catalytic tests, adsorption tests and SER tests. Also, the process indicators used for performance assessment and comparison are described.

Chapter 4 presents the results and respective discussion. After assessing the performance of catalysts and one zeolite on methanation and water adsorption, respectively, the results obtained using the adsorptive reactor are presented and the main advantages of its use are discussed.

Chapter 5 presents the main conclusions of the work.

Chapter 6 offers an evaluation of the developed work and presents recommendations for future activities.

# 2 Context and State of the art

As mentioned in the previous chapter, the methanation reaction is exothermic and occurs, usually, between 200 and 550 ºC, depending on the catalyst in use. For that reason, high temperatures are thermodynamically unfavorable for the Sabatier reaction. Pressure also plays a crucial role, being that high pressures favor the forward reaction, from the thermodynamic viewpoint, due to the decrease of the number of moles. Figure 2.1 shows the $CO_2$ conversion as a function of temperature and pressure in the thermodynamic equilibrium [12].

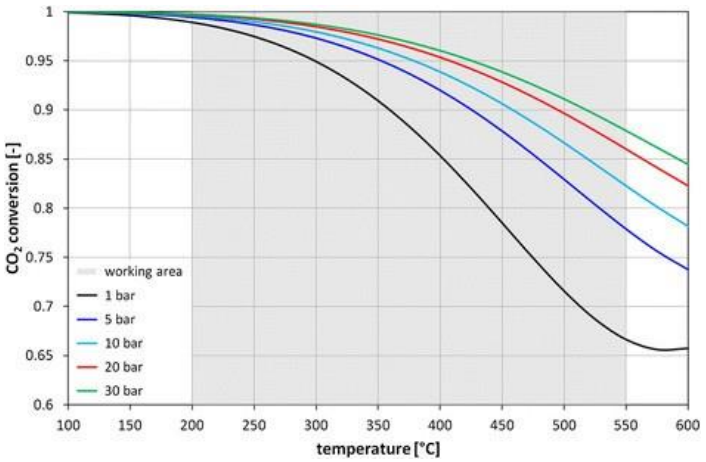



*Figure 2.1. Temperature and pressure influence on $CO_2$ conversion (for $H_2/CO_2 = 4$), extracted from [13].*

Besides temperature and pressure conditions, the methanation reaction is also influenced by the catalyst. In the specific case of the sorption-enhanced reactor (SER) addressed in this thesis, there is also the need to take into account the behaviour of the water adsorbent [7, 14]. Both types of materials will be addressed in the subsequent sections.

## 2.1 Methanation Catalysts

Catalysts are materials that are not consumed during the reaction but allow the increase of the reaction rate. Their main roles include decreasing the activation energy, decreasing the reactant requirement (to obtain a given amount of product) and being selective towards specific products [15]. Most of the research on methanation catalysts is related to the improvement of their activity, selectivity, stability and cost-effectiveness [16].

Methanation catalysts are usually composed of active metal particles, such as Ni, Fe, Co, Ru, Rh, Pt and Pd, dispersed on metal oxide supports like $Al_2O_3$, $SiO_2$, $TiO_2$ and $CeO_2$ [16]. Although noble metals have shown to be more active, especially at lower temperatures, transition metals

are cheaper while still presenting considerable activity and higher $CH_4$ selectivity, which makes them an attractive option for industrial-scale processes [17].

Hence, although particularly ruthenium presents high activity and produces almost exclusively $CH_4$, nickel-based catalysts are widely studied due to their good activity, availability, and lower price. However, one disadvantage of this kind of catalysts is the requirement of higher temperatures, resulting in lower stability and inherently reduced catalyst lifetime; still, their use hinders obtaining high $CO_2$ conversions at low temperatures [18, 19].

One of the big challenges in catalysis and also for methanation is catalyst chemical or physical deactivation. Chemical deactivation can occur through poisoning, caused, for example, by the presence of $H_2S$, and results in the blocking of active sites available for the catalytic reaction or in the modification of the chemical nature of the catalyst. On the other hand, physical deactivation usually occurs through thermal degradation or fouling [16, 20]. Usually, high temperatures and pressures cause the catalyst activity and lifetime to quickly reduce; so, being a strongly exothermic reaction, methanation is partially responsible for the catalyst deactivation, increasing the sintering effects, i.e., the loss of surface area [21, 22].

Catalyst coking occurs usually as a consequence of $CO_2$ dissociation into CO and coke formation, through de Boudouard reaction [23]. This phenomenon is more problematic in nickel catalysts because of the lower water concentration on the active sites and is related to the Ni particle size [24, 25]. Efforts to overcome this issue are being made and there is evidence that the coking is highly dependent on the dispersion of Ni nanoparticles, being this drawback able to be controlled by using additives to enhance metal-metal and metal-support interactions [26]. For example, Ramezani *et al.* [27] studied the effect of Mg addition in a Ni-Mn/$Al_2O_3$ catalyst and observed an increase in nickel dispersion, resulting in less carbon deposits. Also, experiments showed that the addition of Co to Ni catalysts improves the reducibility of nickel species while also improving activity and selectivity towards $CH_4$ [28]. Lu *et al.* [29] conducted a study on the introduction of Fe, Co, Ce and La in a nickel catalyst supported on zirconia, concluding that the presence of the latter prevents the formation of nickel nanoparticles. Also, the presence of the additives reduces nickel species and grants higher thermal stability for $CO_2$ methanation.

Catalyst performance is affected by the interaction metal-support. Some of the commonly used supports for Ni catalysts include the aforementioned, as well as zeolites and hydrotalcites. A study on several Ni supported catalysts showed high dependence of catalytic activity for $CO_2$ methanation on the existence of moderate basic sites in the catalyst [30, 31]. Regarding the use of zeolites as catalyst support, a study showed $CO_2$ conversions above 70 % for temperatures above 400 ºC and increased $CH_4$ selectivity for increasing Ni contents [32].

Fu *et al.* [33] studied the methanation reaction using $Ni/ZrO_2$-$Al_2O_3$ obtaining 84.4 % $CO_2$ conversion and almost 100 % $CH_4$ selectivity at 280 ºC. An experiment with $Ni/CeO_2$-La provided approximately 90 % of $CO_2$ conversion and nearly 99 % of methane selectivity at 300 ºC. Other studies on Ni catalysts with various supports showed high $CO_2$ conversion and almost 100 % $CH_4$ selectivity in the low temperature range (200-300 ºC), revealing some Ni-based catalysts as a good option for low temperature methanation [18, 34].

## 2.2 Water Adsorbents

Adsorption is a separation process through which a molecule is transferred from a bulk (adsorbate) to a solid surface (adsorbent), the latter usually being a porous material due to the high surface area or high micropore volume. Adsorption can occur through three different mechanisms: i) steric, based on the different dimensions of the pores and the molecules to be adsorbed, ii) equilibrium, based on the different abilities of the adsorbent to accommodate different species, and iii) kinetic, based on the diffusion rates into the pores [35, 36].

This mass transfer phenomenon may be physical or chemical, depending on the adsorption forces involved. Physical adsorption occurs through intermolecular forces, such as van der Waals, resulting in weak interactions that allow easy reversibility. It usually happens at low temperatures with fast adsorption rate and physically adsorbed molecules do not bound to specific locations of the adsorbent surface. Chemical adsorption is a highly selective process and occurs only between certain adsorptive and adsorbent species as it requires the share of electrons to form a covalent bond. As is it a stronger “connection”, it is more difficult to reverse [37], and involves higher enthalpies of adsorption, in the range of -80 to -200 $kJ \cdot mol^{-1}$ (whereas for physical adsorption the enthalpy value is around 0 and -20 $kJ \cdot mol^{-1}$ [38]).

The amount of adsorbate retained in the adsorbent is dependent on the specific surface area of the adsorbent, the size of the adsorbate molecule and the interaction(s) between them, caused by polarity or by the equilibrium temperature and pressure [39].

As the adsorption process proceeds, the sorbed solute (adsorbate) tends to desorb into the solution (bulk) and, at some point, the rates of adsorption and desorption are equal, reaching an equilibrium state. At the adsorption equilibrium, the amount adsorbed attains a maximum and no change in solute concentration can be observed on the solid surface. The equilibrium position depends on the characteristics of the adsorbent and the adsorbate, temperature, and partial pressure [40].

The amount adsorbed can be presented in isobars, i.e. at constant pressure, isosteres, i.e. at constant amount adsorbed, or as isotherms, i.e. at constant temperature. The latter are the most used to characterize the equilibrium adsorption and express the amount adsorbed, at a specific temperature, as a function of the partial pressure of the adsorbent, $p_i$, up to the

saturation pressure, $p_s$. As already mentioned, temperature and pressure affect the adsorption capacity and, as a consequence, the amount adsorbed in the equilibrium, $q_{eq}$, is also a function of these two variables. The amount adsorbed can be defined as described by Equation 2.1 [41].

$$q = \frac{adsorbed\ moles}{mass\ of\ adsorbent} \tag{2.1}$$

In a continuous process, adsorption may occur on a column (packed-bed with adsorbent) where the adsorbates flow. The feed might be, for instance, a step function, and adsorption begins at the entrance of the column and progresses to the exit. Over time, a zone at the beginning of the column starts to saturate and that zone evolves until the end of the column. For this kind of saturation process, the exit concentration is usually represented as shown in Figure 2.2 and these concentration-time curves are commonly referred to as breakthrough curves. From this type of curves, it is possible to conclude if the adsorption is poor or strong [40, 42].

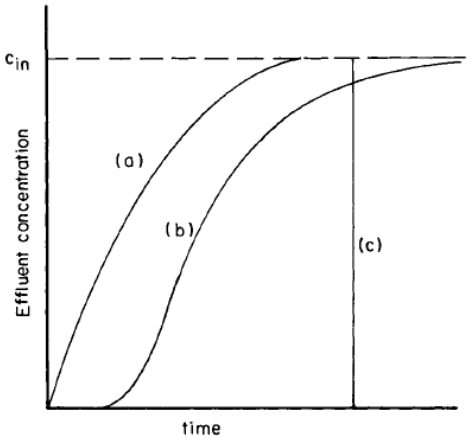



*Figure 2.2. Examples of breakthrough curves: (a) - poorly adsorbed; (b) – commonly cases, (c) - strongly adsorbed with no mass-transfer effect, extracted from [40].*

After the adsorption step, there is the need to regenerate the adsorbent so that its adsorption capacity is re-established, and it can be used again. The regeneration step can be done through an increase in temperature (TSA – thermal swing adsorption), a decrease in pressure (PSA - pressure swing adsorption), by using an inert stream through the adsorbent (displacement desorption), with a chemical reagent that changes the adsorbent characteristics, with strong solvents or by decomposition. For gases, desorption is usually made by an inert stream, PSA or TSA [43].

The most commonly studied water adsorbents include activated carbon, activated alumina, silica gel, zeolites and, more recently, metal-organic frameworks (MOFs) [43].

Being an exothermic process, adsorption is favored, from a thermodynamic point of view, at low temperatures and high pressures. However, the high temperature required for the Sabatier

reaction to occur (between 200 and 550 ºC, as mentioned before) and the fact that it is an exothermic reaction, can affect the performance of the water adsorbent if both (methanation catalyst and water adsorbent) are coupled together in a SER. Hence, in order to guarantee the best adsorption capacity possible, it is mandatory that the adsorbent presents high affinity for water [9]. Besides that, high temperature can also play a role on the adsorbent decomposition as, for example, silica gel starts to decompose at around 300 ºC, reason why there is little information on the literature for its use in high-temperature adsorption [44].

However, studies on some zeolite molecular sieves, like Linde Type A and Faujasite zeolites, showed good adsorbent capacity for high temperatures, thermal stability, and desorption only above 220 ºC. Thus, there is evidence to believe that zeolites are a good adsorbent option to apply along with the methanation process. Besides that, they can also be used as catalyst support, and thus as dual function materials (with both catalytic and adsorption properties) [9, 45, 46].

Zeolites are porous crystalline aluminosilicates of alkaline or alkali earth metals that have a uniform structure of pores, which can be in form of pellets, beads or powder [47]. There are 30 kinds of zeolites that exist in natural mines but they can be produced industrially, being the most commonly used type A (LTA) and Faujasite (type X and Y) [48].

In this category of adsorbents, internal and external adsorption occurs depending on the size of the adsorbate molecules and the pore diameter of the zeolite. If the size of the adsorbate molecule is inferior to the pore diameter and this pore area is available, internal adsorption occurs. If the size of the adsorbate molecule is superior to the pore diameter, the adsorbate can be adsorbed at the external surface, though at maximum occupying 1 % of the total surface area [49].

There are some studies on water adsorption at high temperatures. Simo *et al.* [50] studied the breakthrough for a water stream in zeolite 3A concluding that the breakthrough time decreases with an increase in temperature, as can be observed in Figure 2.3, due to the decrease in bed capacity. This temperature dependency is related to the presence of micropore diffusion mechanism. Besides that, it was verified that mass transfer is controlled by the diffusion in micropores, being macropore diffusion more relevant at higher temperatures.

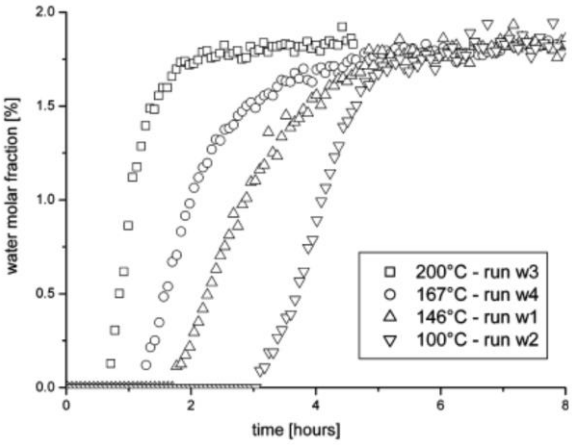



*Figure 2.3. Adsorption breakthrough curves of water on 3A zeolite at different temperatures, extracted from [50].*

Also, a study on molecular sieve 3A showed increasing adsorption capacity at higher pressure and adequate adsorption performance of zeolite 3A at elevated temperatures (200-350 ºC) [48].

Considering the goal of introducing the adsorbent in a sorption-enhanced reactor, it is important to consider the possibility of the zeolite to adsorb other species besides water. Hence, Wang and LeVan [51] determined $CO_2$ isotherms on zeolites 5A and 13X for a temperature range of -45 ºC to 175 ºC, as well as for $H_2O$ between 0 ºC and 100 ºC, verifying that the sorption capacity was greater for water than for carbon dioxide for the two zeolite types, being slightly higher for zeolite 5A. Besides that, Walspurger *et al*. [9] studied zeolite 4A adsorption performance in a temperature range of 200 to 300 ºC and $p_{CO_2}$ of 0.025 bar and concluded that, despite the negligible sorption capacity towards $CO_2$, its presence reduced the water sorption capacity by about 15-20 %.

## 2.3 Sorption-Enhanced Reactor

The sorption-enhanced reactor (SER) is the main focus of this work and appears as a possible solution to enhance the methanation process by combining two chemical processes in one reactor. The SER is, thus, a result of process intensification, i.e., the application of innovative principles applied in process and equipment design with the goal of lowering the process expenses while still improving the process performance and products quality, and is considered a multifunctional reactor as it combines chemical reaction and adsorption in one unit [52-54]. Besides the combination of reaction and products separation, a multifunctional reactor can combine reaction and heat transfer and even several reactions. There are already some processes in which multifunctional adsorptive reactors have been used, including steam methane reforming, water-gas shift and the Claus process [55].

The sorptive reactor focused in this work requires a mix of a methanation catalyst and a water adsorbent that must be chosen wisely as they must be able to be used in the same conditions. This might represent an issue as catalyst activation might require high temperatures, not favourable for the adsorption. Hence, noble metals appear as a good option for the sorptive reactor; however, as mentioned above, their high prices make them an unfeasible option at the industrial level, implying the search for other solutions.

The mix of catalyst and adsorbent can be displayed in the reactor randomly or in alternating layers. Another option is to use an hybrid material with adsorbent and catalytic properties, also called a sorption catalyst or dual function material [56]. By promoting greater proximity between adsorbent and catalytic sites and reducing mass transport limitations, the sorption catalyst presents itself as a better option [57]. Figure 2.4 shows a schematic representation of a traditional reactor and a sorption-enhanced reactor, with a random mixture of catalyst and adsorbent.

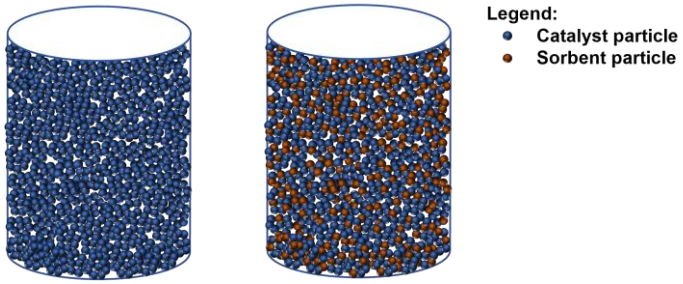



*Figure 2.4. Schematic representation of a traditional reactor (on the left) and a SER (on the right).*

By using the adsorbent during the methanation reaction it is possible to capture one of the reaction products, shifting the equilibrium forward and improving the reaction kinetics. However, as previously mentioned, after the adsorption step, the adsorbent requires a regeneration step, otherwise the sorption-enhancement effect becomes less effective, and the SER ends up working as a traditional packed-bed methanation reactor. A pressure or temperature swing adsorption (PSA/TSA) reactor with an adsorbent and catalyst in a fixed bed can be used in this process [58]. To attain continuous operation there is the need to use more than one sorption reactor. If the saturation and regeneration times are equal, a continuous process with two units may be possible, but desorption is often the limiting step taking more time to complete, defining the time of the cycle [57].

Applying the SER to the biogas upgrading allows the use of a single chemical unit for simultaneous water separation and conversion of $CO_2$ while shifting forward the reaction equilibrium. Besides that, there is evidence that in-situ water removal reduces the amount of carbon oxides in the outlet stream, thus increasing methane selectivity and allowing the obtention of a biogas stream able to be injected in the natural gas grid[59]. For these reasons,

there are already a few studies revealing the advantages of using a sorptive reactor for the methanation process, as summarized herein below.

Walspurger *et al.* [9] used nickel-based catalysts and zeolite 4A for methanation and observed great advantages of using the sorption-enhanced reactor for lower pressures (below 10 bar), namely the possibility of obtaining a methane stream that meets the needed requirements for injection into the grid combined with a reduction in the energy required for compression of the same stream, allowing for a reduction in costs. It was also concluded that water sorption capacity decreases with an increase of the adsorption temperature, as expected.

Borgschulte *et al.* [8] also tested a SER using sorption catalysts based on Ni particles in zeolite 5A. From the experiments it was possible to conclude that the adsorption enhancement effect is more noticeable for intermediate conversions, although 100 % $CH_4$ selectivity was obtained for all studied temperatures (150-300 ºC). Nevertheless, the need for a nanostructured sorption catalyst was emphasized.

A study to compare zeolites 5A and 13X was performed on a SER using a nickel-based catalyst at 300 ºC and allowed to conclude that zeolite 13X has higher water sorption capacity than 5A [45]. Nevertheless, both zeolites allowed to obtain complete $CO_2$ conversion and 100 % of selectivity for methane at 300 ºC during the sorption-enhanced mode. Figure 2.5 shows the $CO_2$ conversion after the adsorbent saturation, i.e., for the traditional methanation; it allows to conclude that, regardless of the adsorbent in use, the average conversion achieved is the same, meaning that it is only dependent on the catalytic phase.

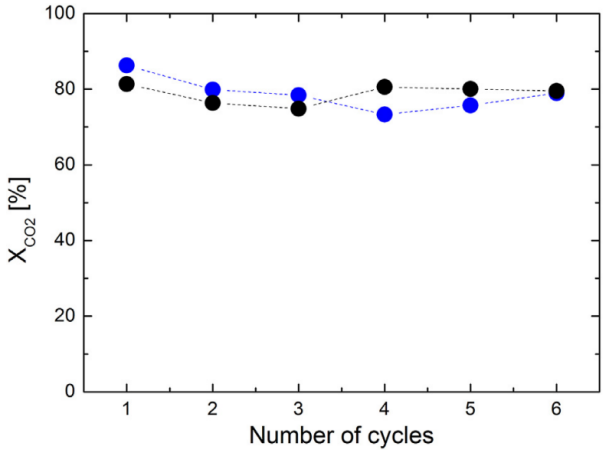



*Figure 2.5. $CO_2$ conversion achieved after adsorbent saturation for 5Ni/5A (blue) and 5Ni/13X (black) at 300 ºC, extracted from [45].*

Also, cyclic tests were performed and showed no influence of the drying time (i.e., adsorbent regeneration) on the adsorption performance, considering that doubling the regeneration time produced no significant effect on the normalized time of operation (NTO), defined as the

product between the time of operation under sorption-enhanced mode and the ratio between the flow rate and the reactor volume. Figure 2.6 shows the experimental results for such a reactor at a temperature of 300 ºC and 20 minutes of drying step (except between cycles 5 and 6, where the drying step was carried out for twice as long), using $H_2$ for the first three cycles and air for the remaining ones [45]. In the figure, it is noticeable a significant higher NTO for the first cycle, justified by the sample pre-treatment that led to a higher reduced nickel phase.

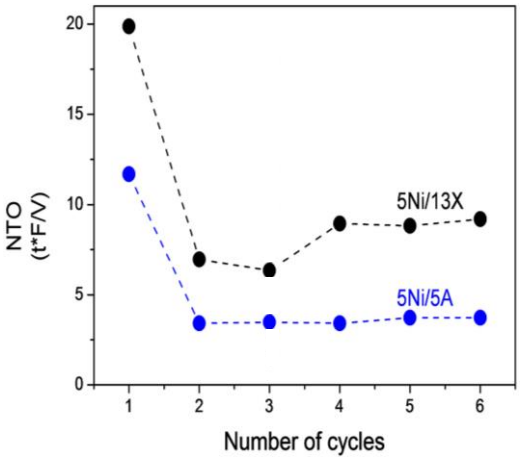



*Figure 2.6. Normalized time of operation (NTO) as a function of the number of cycles, adapted from [45].*

# 3 Materials and Methods

## 3.1 Catalytic tests

The catalytic tests were performed using three commercial catalysts sieved into particle sizes in the range of 350-600 µm, namely 0.5 % $Ru/Al_2O_3$ (supplied by Aldrich), $NiO/Al_2O_3$-$SiO_2$-CeO (supplied by REB Research and Consulting) and Sample 3 (supplied by an European Catalyst Supplier, not disclosed herein for confidential reasons).

A scheme of the experimental setup used for the catalytic tests is represented in Figure 3.1.

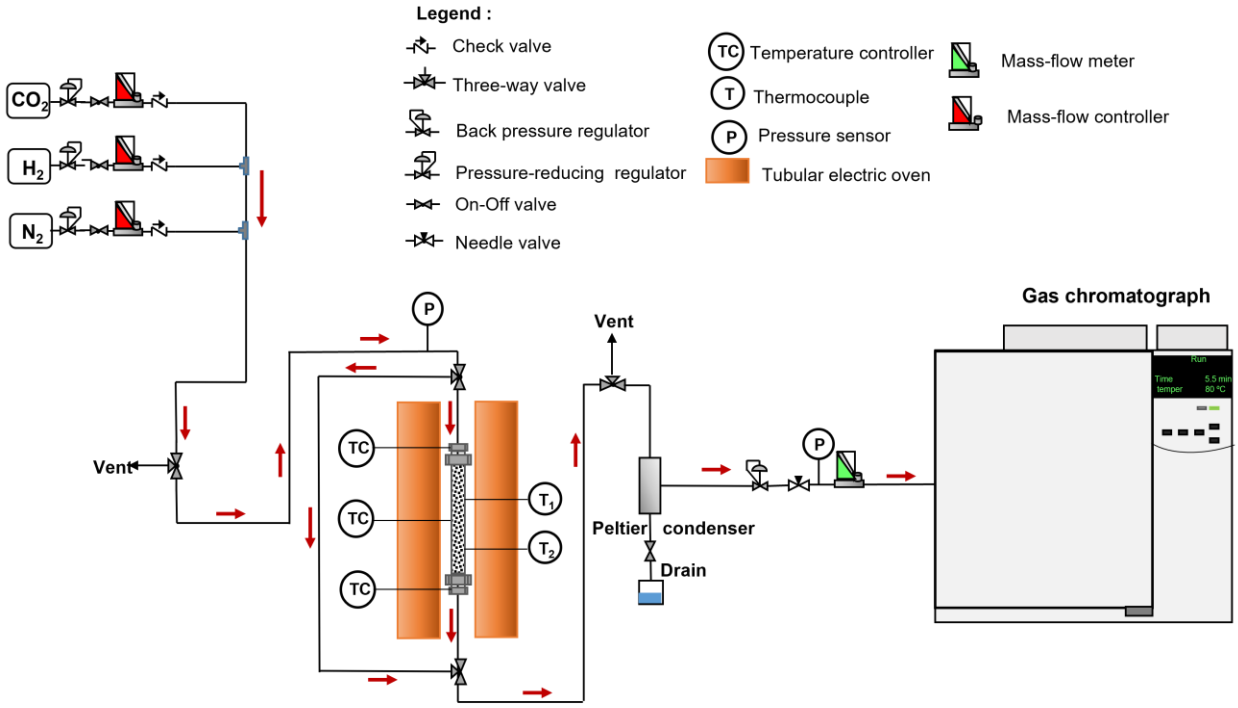



*Figure 3.1. Scheme of the experimental setup for the catalytic tests, adapted from [60].*

The feed gases ($H_2$, $CO_2$ and $N_2$), supplied by Air Liquide with 99.9995 %, 99.998 % and 99.999 % purity, respectively, were fed to a fixed-bed reactor, consisting of a stainless steel 120 mm long tube with an inner diameter of 7.2 mm, after passing through the respective mass flow controllers (model 201, from Bronkhorst Hi-tec). The reactor was placed inside a tubular electric oven (from Termolab) equipped with three PID temperature controllers (TC) connected to three type-K thermocouples. The temperature inside the reactor was measured by two type-K thermocouples (T) radially placed in direct contact with the catalytic bed, 40 and 80 mm from the reactor inlet.

The experimental installation also consists of a by-pass to the reactor, necessary for the calibration of the analysis equipment, namely in the determination of the reference areas regarding the use of the chromatograph.

In order to prevent steam condensation, the outlet reactor tubes were heated and thermally isolated with glass wool. The outlet of the reactor contained water vapor that was condensed using a Peltier cooler.

The dry stream composition was determined online using a gas chromatographer (Agilent model 7820A) equipped with a pair of detectors, a TCD (Thermal Conductivity Detector) and a FID (Flame Ionization Detector), and two columns, Plot Q (30 m × 0.32 mm) and Plot 5A (30 m × 0.32 mm). Due to the higher difference in thermal conductivity, the TCD was used with argon as carrier gas, resulting in better $H_2$ analysis. Also, the chromatograph was equipped with a methanizer that allowed the direct $CH_4$ analysis in the FID, by converting CO and $CO_2$.

The catalysts' performance was expressed through $CO_2$ conversion ($X_{CO_2}$) and $CH_4$ selectivity ($S_{CH_4}$), obtained according to Equations 3.1 and 3.2,

$$X_{CO_2}(\%) = \frac{F_{CO_{2_{in}}} - F_{CO_{2_{out}}}}{F_{CO_{2_{in}}}} \times 100\ \% \tag{3.1}$$

$$S_{CH_4}(\%) = \frac{F_{CH_{4_{out}}}}{F_{CH_{4_{out}}} + F_{CO_{out}}} \times 100\ \% \tag{3.2}$$

where $F_{i_x}$ is the molar flow rate of component $i$ in steam $x$: inlet or outlet of the reactor. The carbon mass balance was calculated for all the tests carried out, being the error always lower than 10 %.

The equilibrium $CO_2$ conversion for all temperatures, pressures and feed compositions studied was calculated using the Gibbs free energy minimization method in the Aspen Plus V12.1 software.

Initially, for each experiment, the reactor was filled with 0.2 g of catalyst and inert (silicon carbide powder – SiC) in a mass proportion of 0.1:3. In addition, the reaction bed contained inert at the beginning and at the end.

Prior to the experiment, the catalyst went through a reduction process with a mixture of 10 mLn·min$^{-1}$ of $H_2$ and 90 mLn·min$^{-1}$ of $N_2$ for 4 hours at temperatures defined by temperature-programmed reduction (TPR) analysis (check Figure 3.2) and presented in Table 3.1. The catalytic tests were performed at 200, 250, 300 and 350 °C and 1 bar using a mixture of 10 mLn·min$^{-1}$ of $CO_2$, 40 mLn·min$^{-1}$ of $H_2$ and 50 mLn·min$^{-1}$ of $N_2$.

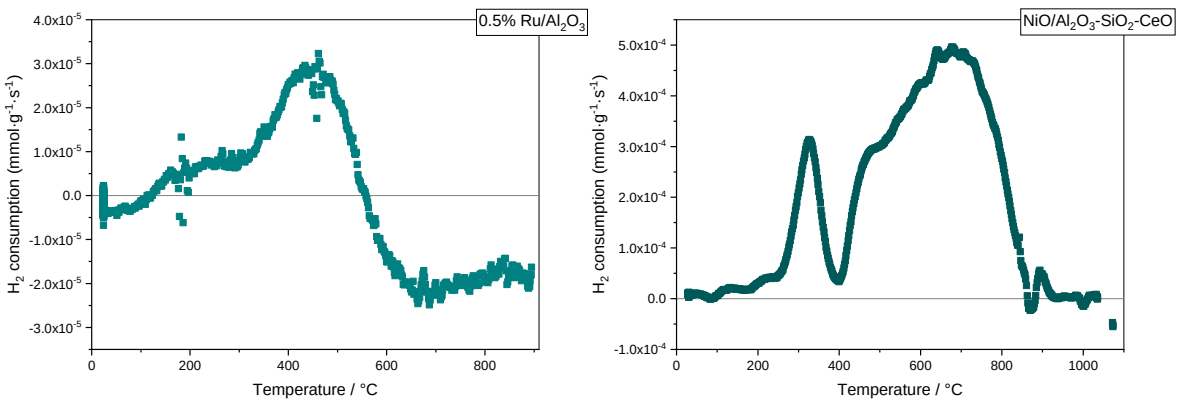



*Figure 3.2. TPR-$H_2$ results for two catalysts: 0.5 % $Ru/Al_2O_3$ (on the left) and for $NiO/Al_2O_3$-$SiO_2$-CeO (on the right)[a].*

Observing Figure 3.2, regarding the ruthenium-based catalyst (on the left), the peak of $H_2$ consumption occurs around 500 °C; however, based on tests previously developed in the working group, and in order to avoid the ruthenium decomposition, it was decided that this catalyst would be reduced at 350 °C. Regarding the Ni-based catalyst, the reduction temperature was assumed to be the one for which the highest hydrogen consumption was observed, around 650 °C.

*Table 3.1. Reduction temperature used for each catalyst.*

| Catalyst | Reduction Temperature / °C |
|---|---|
| 0.5 % $Ru/Al_2O_3$ | 350 |
| $NiO/Al_2O_3$-$SiO_2$-CeO | 650 |
| Sample 3 | 550[b] |

The catalytic performance was evaluated for these 3 samples and the most promising one was used to study the influence of several parameters, including reduction temperature, gas velocity, total pressure and feed composition. Table 3.2 presents a summary of the operating conditions for each test.

[a] The results were obtained and provided by Cristina Caeiro.

[b] Temperature defined by manufacturer's recommendation.

*Table 3.2. Operating conditions used in the experimental tests, for $WHSV_{CO2}$ = 3 Ln·g$^{-1}$·h$^{-1}$.*

| Parameter | Reduction Temperature / °C | Mass of catalyst / g | Feed composition ($CO_2$/$H_2$/$N_2$) / mLn·min$^{-1}$ | Temperature / °C | Pressure / bar |
|---|---|---|---|---|---|
| **Reduction Temperature** | **650; 800** | 0.20 | 10/40/50 | 200; 250; 300; 350 | 1 |
| **Gas Velocity*** | 650 | 0.10; 0.20; 0.25 | 5/20/25; 10/40/50; 12.5/50/62.5 | 200; 250; 300; 350 | 1 |
| **Total Pressure** | 650 | 0.20 | 10/40/50 | 200; 250; 300; 350 | **1; 4; 6** |
| **Feed Composition** | 650 | 0.20 | **10/40/50; 10/40/0** | 200; 250; 300; 350 | 1 |

*Contact time was kept constant as $WHSV_{CO_2} = \frac{Q_{CO_2}}{m_{cat}} = constant = 3\ Ln \cdot g^{-1} \cdot h^{-1}$.

## 3.2 Adsorption tests

Taking as reference previous studies of the group[c], zeolite 13X (Grace - Sylobead MS C 548 BATCH NO 1000362450) was used to perform the water adsorbent characterization tests. Prior to the experiments, the zeolite was sieved into 350-600 µm.

A scheme of the experimental setup used for the adsorption tests is represented in Figure 3.3.

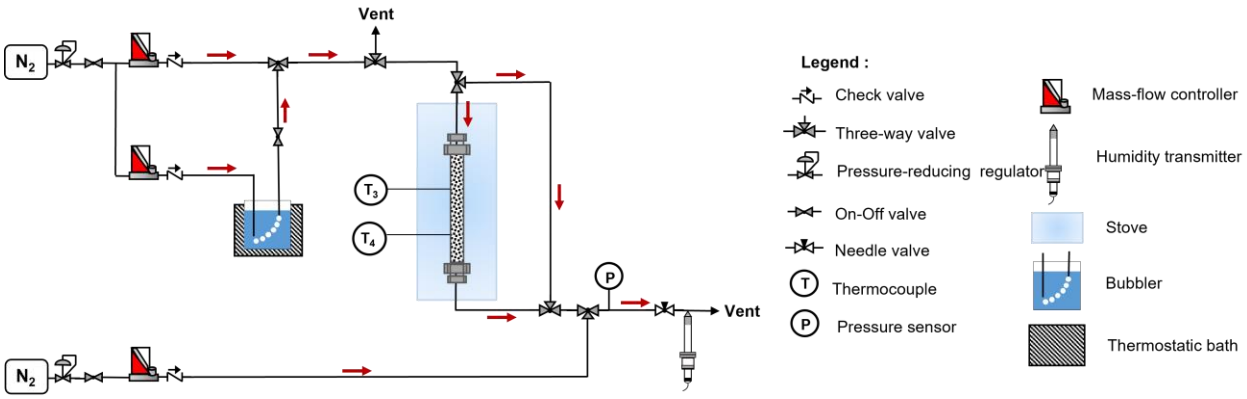



*Figure 3.3. Scheme of the experimental setup for the adsorption tests.*

[c] The results were obtained and provided by Cristina Caeiro.

The tests were carried out in a fixed-bed tubular device, similar to the one used in section 3.1 (120 mm long and with an i.d. of 7.2 mm), equipped with two type-K thermocouples for temperature reading and placed inside an oven (model UNB 100, from Memmert).

In order to study water adsorption, the column was fed with a mixture of two nitrogen-based streams, a pure one (100 mLn·min$^{-1}$) and a water vapor saturated one. The latter is obtained by passing a nitrogen stream (100 mLn·min$^{-1}$) through a bubbler filled up with an appropriate amount of distilled water, which is placed inside a thermostatic bath at 25 °C. Pure nitrogen (200 mLn·min$^{-1}$) is used for the regeneration step, and to flush the piping. All the flow rates are controlled by mass flow controllers (model 201, from Bronkhorst Hi-tec).

The column outlet stream passes through a humidity transmitter (model HMT310, from Vaisala) to determine the stream humidity and, subsequently, the amount of water adsorbed.

The adsorbent performance was analysed according to the amount of water adsorbed until the adsorbent was saturated, i.e. the time after which the amount of water on the outlet is the same as in the inlet, determined as the area above the experimental breakthrough curve (until that point) and obtained through Equation 3.3,

$$q_{H_2O} = \frac{F_{H_2O_{in}} \int_0^t \left(1 - \frac{y_{H_2O_{out}}}{y_{H_2O_{in}}}\right) dt}{m_{ads}} - q_{H_2O,blank} \tag{3.3}$$

where $F_{H_2O_{in}}$ is the molar flow of water in the inlet, $y_{H_2O_{in}}$ and $y_{H_2O_{out}}$ are the molar fraction of water in the inlet and outlet streams, respectively, $m_{ads}$ stands for the mass of adsorbent used, and $q_{H_2O,blank}$ represents the amount adsorbed in a blank test in which the column was filled only with inert (SiC).

Prior to the experiments, the packed bed with adsorbent went through a “cleaning” or regeneration step, with a nitrogen flow rate of 200 mLn·min$^{-1}$ at 300 °C for 4 hours. The experiments were then performed at the temperature of interest, determined according to the results obtained in the catalytic tests, 250 °C, at a total pressure of 1, 4 and 6 bar, in three cycles of adsorption (until saturation) and regeneration for each pressure, so that the cyclical stability could be assessed. The adsorption step was performed using 100 mLn·min$^{-1}$ of pure $N_2$ and 100 mLn·min$^{-1}$ of water-saturated $N_2$ while the desorption step was performed using a flow rate of 200 mLn·min$^{-1}$ of $N_2$.

## 3.3 SER tests

To perform the sorption-enhanced reaction tests, the most promising catalyst from the screening was used, mixed with zeolite 13X.

The experimental setup used for these tests is very similar to the one used in the catalytic tests and is presented in Figure 3.4. The only difference is that the composition of the dry outlet stream was measured using not only the gas chromatograph, but also an online infrared-based $CO_2$ and CO analyser (model 4210, from Servomex), in order to allow a continuous measurement over time.

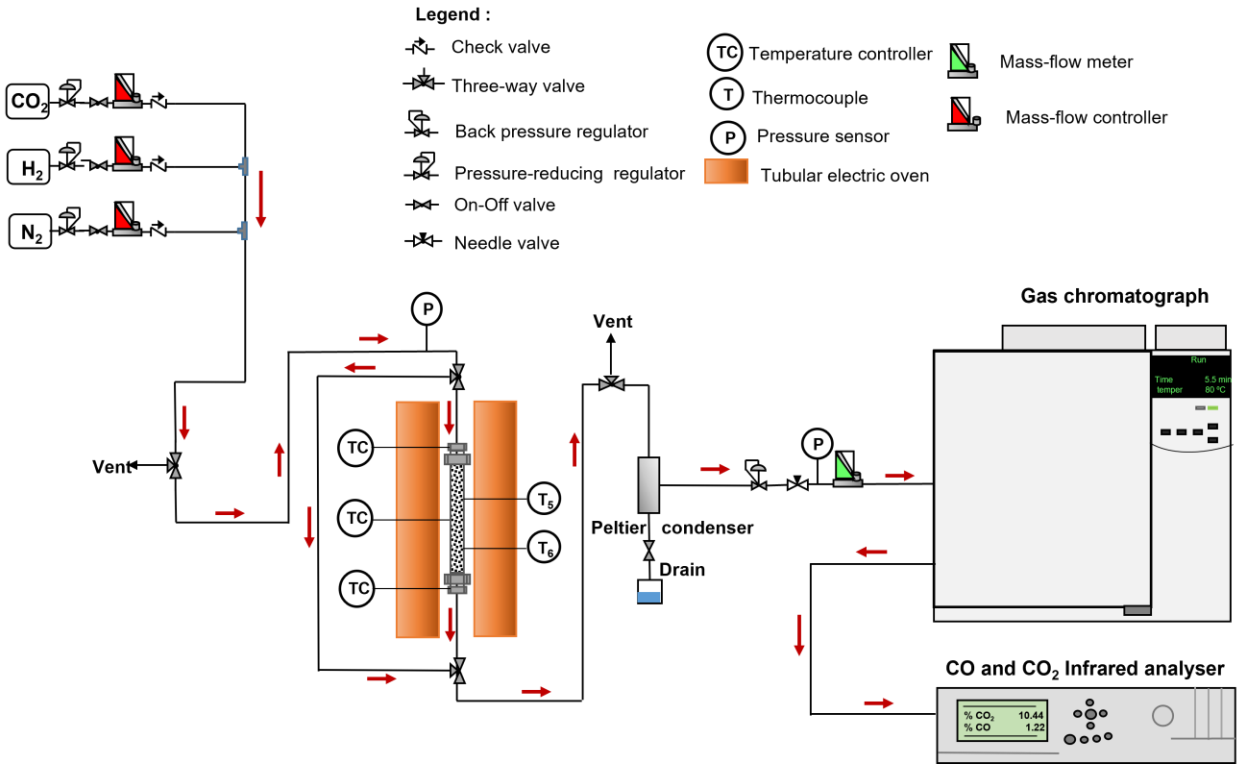



*Figure 3.4. Scheme of the experimental setup for the SER tests, adapted from [60].*

The tests were performed using a fixed-bed reactor, with the dimensions aforementioned, filled with 0.2 g of catalyst, 3.5 g of adsorbent and inert. Prior to the tests, a reduction step was performed in order to activate the catalyst using a mixture of 10 mLn·min$^{-1}$ of $H_2$ and 90 mLn·min$^{-1}$ of $N_2$ for 4 hours at the reduction temperature of the catalyst in use (check Table 3.1). The tests were performed at 250 °C and 1, 4 and 6 bar until saturation of the zeolite was achieved, using a using a mixture of 10 mLn·min$^{-1}$ of $CO_2$, 40 mLn·min$^{-1}$ of $H_2$ and 50 mLn·min$^{-1}$ of $N_2$.

Using the same reactor fill, and a mixture of 7 mLn·min$^{-1}$ of $CO_2$ and 93 mLn·min$^{-1}$ of $N_2$, $CO_2$ adsorption was studied at 250 °C and 4 bar.

In order to understand if the zeolite had catalytic activity over the reactional mixture, a test using a reactor filled only with 3 g of zeolite 13X was performed at 250 °C and 4 bar; the reactor was fed with 10 mLn·min$^{-1}$ of $CO_2$, 40 mLn·min$^{-1}$ of $H_2$ and 50 mLn·min$^{-1}$ of $N_2$. Before the test,

the zeolite was heated up to 300 °C for 4 hours, while a nitrogen flow of 100 $mLn \cdot min^{-1}$ was passing, to ensure that it was completely free of water.

Finally, in order to correct the acquisition time of the Servomex, considering the delay in the equipment response, blank tests were performed, using a reactor filled only with inert, at 250 °C and 1, 4 and 6 bar. The same reactional mixture described above was fed to the reactor.

# 4 Results and discussion

## 4.1 Catalytic tests

### 4.1.1 Catalytic screening and effect of reaction temperature

The results of the tests performed with each catalyst, for the evaluation and comparison of their performance, are presented in Figure 4.1. The reduction temperatures can be checked in Table 3.1. The feed was composed of 10 vol. % $CO_2$, 40 vol. % $H_2$ and 50 vol. % $N_2$.

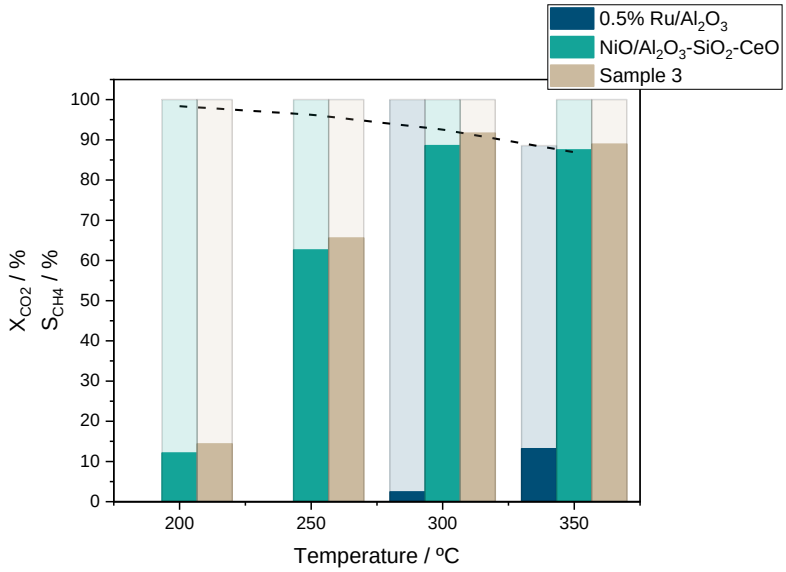



*Figure 4.1. Effect of temperature in $CO_2$ conversion for P = 1 bar, $WHSV_{CO2}$ = 3 $Ln \cdot g^{-1} \cdot h^{-1}$ and $H_2/CO_2$ molar ratio = 4. The bars in lighter colours represent the selectivity to methane obtained for each experiment. The dashed line represents the thermodynamic equilibrium.*

Figure 4.1 allows the study on the influence of the reaction temperature on $CO_2$ conversion. For all the catalysts tested, it was found that an increase in the reaction temperature results in an increase in the conversion, due to catalyst activation – higher temperatures accelerate the reaction kinetics, according to the Arrhenius law. This effect is less pronounced for higher temperatures, as these are less favorable for the exothermic Sabatier reaction, leading to a stabilization of $X_{CO2}$ close to the limit imposed by thermodynamics (dashed line).

Comparing the Ru-based catalyst with the Ni-based one and Sample 3, it is possible to conclude that the former exhibited poorer activity. Besides that, selectivity under 100 % was obtained only for the catalyst 0.5 % $Ru/Al_2O_3$ at 350 °C, which was active only for temperatures above 250 °C. Considering the similar $X_{CO2}$ obtained for the remaining catalysts and the greater availability of $NiO/Al_2O_3$-$SiO_2$-CeO, this was chosen for the subsequent tests.

### 4.1.2 Effect of reduction temperature

Considering the previously mentioned TPR results and the fact that usually reduced NiO species present three characteristic TPR peaks: α (200-350 °C), β (300-600 °C) and $\gamma_1$ (500-700 °C) [61], the effect of the reduction temperature on $CO_2$ conversion was studied increasing the reduction temperature to 800 °C, while keeping constant the remaining variables. Figure 4.2 shows the results obtained.

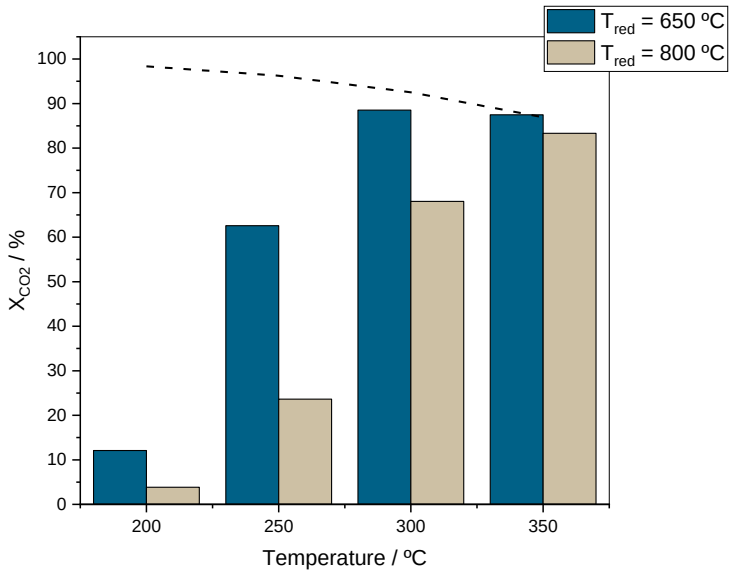



*Figure 4.2. Effect of reduction temperature on $CO_2$ conversion at different temperatures for P = 1 bar, $WHSV_{CO2}$ = 3 $Ln \cdot g^{-1} \cdot h^{-1}$ and $H_2/CO_2$ molar ratio = 4. The dashed line represents the thermodynamic equilibrium.*

Figure 4.2 shows that an increase in the reduction temperature leads to a weaker catalyst performance, resulting in lower $CO_2$ conversions at all temperatures tested. This phenomenon can possibly be explained by the occurrence of catalyst sintering, causing the alteration of the catalyst structure and, consequently, the loss of active sites; characterisation of the used material is however required to check this hypothesis.

### 4.1.3 Effect of gas velocity

Regarding the tests to evaluate the effect of the gas velocity, it is worth noting that for comparison matters, the feed flow rates were adjusted as the mass of catalyst was changed in order to keep the weight hourly space velocity regarding $CO_2$ constant. This way, one is changing the gas velocity, keeping the contact time constant.

The results obtained for the conversion of $CO_2$ as a function of the total flow rate for different temperatures are presented in Figure 4.3.

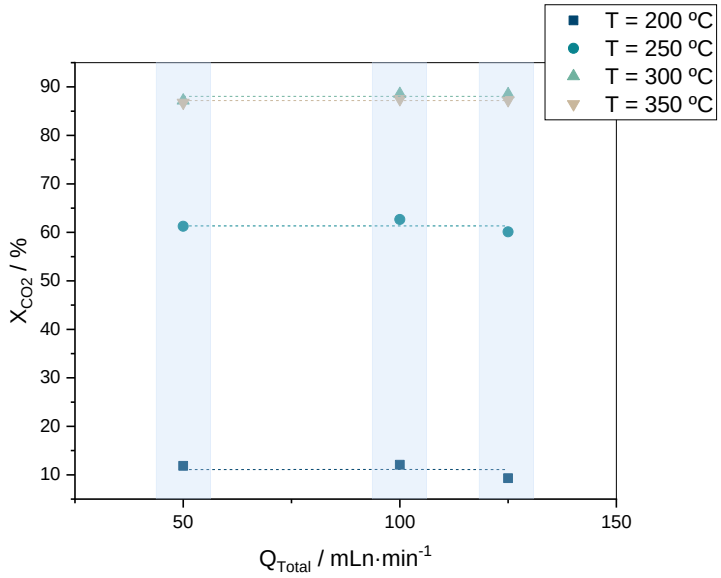



*Figure 4.3. Effect of the gas velocity on $CO_2$ conversion at different temperatures for P = 1 bar, $WHSV_{CO2}$ = 3 Ln·$g^{-1}$·$h^{-1}$ and $H_2/CO_2$ molar ratio = 4. The dashed lines represent the average $X_{CO2}$ obtained for each temperature.*

From the results it is possible to observe that, at constant temperature, a change in gas velocity does not lead to significant changes in $CO_2$ conversion. Hence, it can be stated that, in this range of mass and flow rates, the system behaves without the influence of external mass transfer limitations and, therefore, the reaction performance is not affected.

### 4.1.4 Effect of total pressure

The effect of total pressure is illustrated in Figure 4.4.

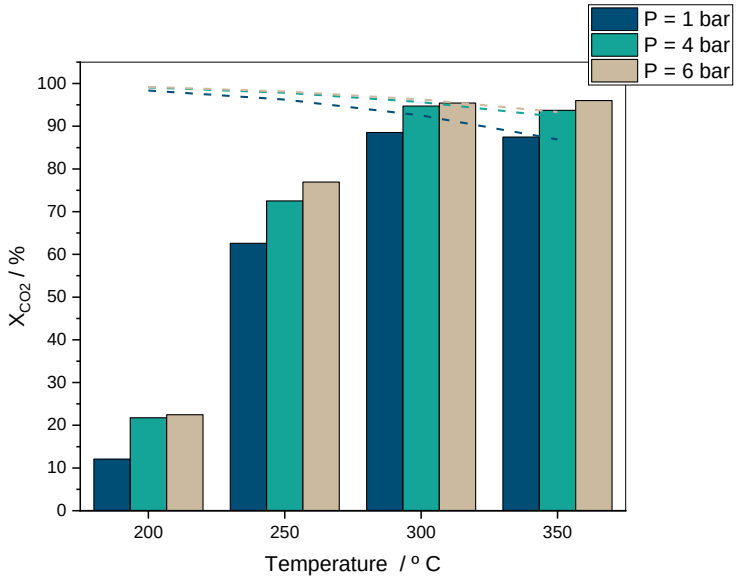



*Figure 4.4. Effect of pressure on $CO_2$ conversion at different temperatures for $WHSV_{CO2}$ = 3 Ln·$g^{-1}$·$h^{-1}$ and $H_2/CO_2$ molar ratio = 4. The dashed lines represent the thermodynamic equilibrium for each pressure.*

Since the methanation reaction leads to a reduction in the number of moles in the reaction system, it is expected that, from the thermodynamic point of view, an increase in pressure favours the reaction; this is shown in Figure 4.4 (see dashed lines). However, experimental data shows increasing $X_{CO2}$ for increasing pressures, at all temperatures under study, even when data are far from equilibrium (200-250 ºC), meaning that total pressure also increases the reaction kinetics. With respect to temperature dependency, regardless of the pressure tested, the effect shown follows the trend already discussed on section 4.1.1, i.e., an increase in $CO_2$ conversion with increasing temperature, due to improved kinetics, and stabilization at 300-350 °C, due to thermodynamic factors.

As a remark, it is worth mentioning that the catalyst proved to be stable at the pressures studied, achieving approximately the same conversions after being submitted to several tests at different pressures. Thus, after a round of tests at different temperatures (200-350 °C) for 1, 4 and 6 bar, the sample was submitted to tests at the same temperatures and at 4 and 6 bar.

### 4.1.5 Effect of feed composition

The effect of the feed composition was evaluated by comparing the reference test (10 % $CO_2$, 40 % $H_2$ and 50 % $N_2$) with one performed without nitrogen (20 % $CO_2$ and 80 % $H_2$). For comparison reasons, all the remaining feed flow rates ($H_2$ and $CO_2$) were kept constant. The results obtained are represented in Figure 4.5.

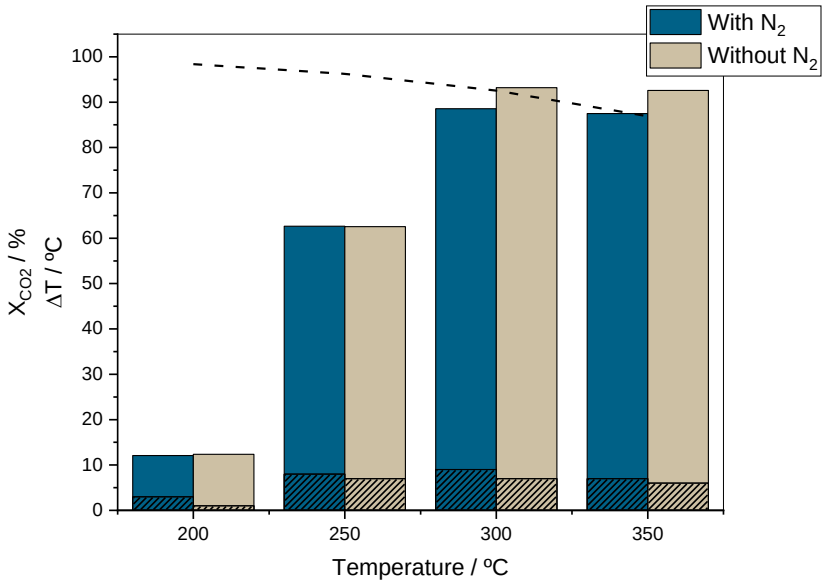



*Figure 4.5. Effect of feed composition on $CO_2$ conversion at different temperatures for P = 1 bar, $WHSV_{CO2}$ = 3 Ln·g$^{-1}$·h$^{-1}$ and $H_2/CO_2$ molar ratio = 4. The dashed line represents the thermodynamic equilibrium. The striped bars represent the temperature increment in the reactor bed at steady state.*

From the figure presented above, it is possible to conclude that the use of the reaction reagents without dilution does not result in significant differences in terms of $CO_2$ conversion.

Also, these tests allowed to study the influence of the inert in the feed stream on the temperature inside the reactor (temperature calculated by the average between the temperatures of the two thermocouples in the reactor). As expected, and as a consequence of the exothermicity of the Sabatier process, in the range of reaction temperatures studied the reaction resulted always in an increase of the reactor temperature, slightly more notorious at temperatures when higher conversions were obtained (300 ºC), regardless the composition of the feed. Furthermore, following the conversion results, no significant differences were observed with the removal of $N_2$ from the feed, being the maximum difference among tests with *vs*. without nitrogen of 2 °C.

## 4.2 Adsorption tests

The adsorption capacity of zeolite 13X was analysed considering the influence of the total pressure and the performance reached throughout the adsorption/desorption cycles. As mentioned above, zeolite 13X was chosen based on previous work carried out at the group, as it presented greater adsorption capacity at the temperature of interest (250 ºC, as $X_{CO2}$ was below $X_{eq}$ for $NiO/Al_2O_3$-$SiO_2$-CeO), when compared to other adsorbents studied (zeolites 3AK, 4ABFK, NaYBFK and 5A). Note that, zeolite 13X showed greater water adsorption capacity for temperatures below 250 ºC; however, at those temperatures, the catalyst was not very active, being uninteresting to study it, with the objective of applying it in the SER.

All the adsorption steps were performed at 250 ºC, while the desorption steps were performed at 300 ºC and 1 bar (for a better and faster regeneration). An example of a breakthrough curve, obtained for a total pressure of 4 bar, is shown in Figure 4.6.

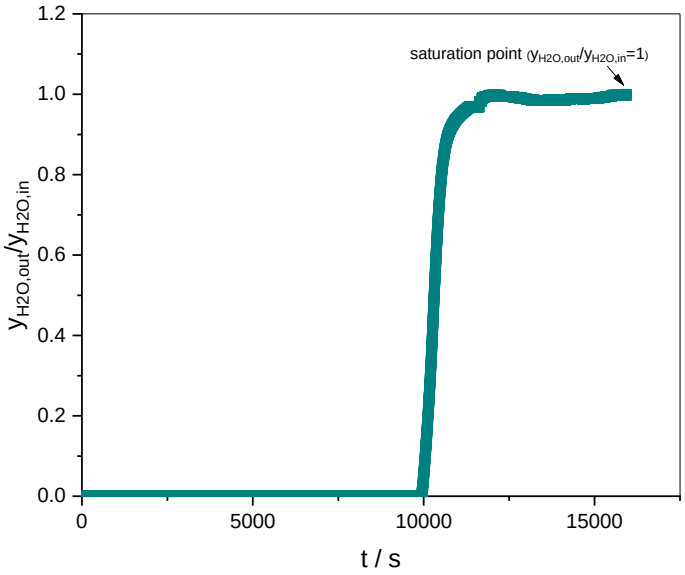



*Figure 4.6. Example of an $H_2O$ breakthrough curve, obtained at 250 ºC and 4 bar, until de saturation point (i.e., $y_{H2O,out}/y_{H2O,in}$=1).*

The adsorption test represented in Figure 4.6 was performed until the saturation point, as can be observed from the figure. That point corresponds to the time in which the amount of water in the outlet matches the amount in the inlet, meaning that the adsorbent is saturated, and no longer adsorbs water. The amount of water in the inlet of the adsorption column was determined experimentally as the maximum measured in the outlet by the humidity sensor.

As mentioned in section 3.2, the water adsorption capacity was calculated as the area above the breakthrough curve, until the saturation point (check Equation 3.3).

The adsorption performance of zeolite 13X was evaluated through its adsorption capacity, at 1, 4 and 6 bar, as well as through its cyclical stability. Therefore, three cycles for each total pressure were performed, and the adsorption capacities obtained were compared.

Table 4.1 contains the $H_2O$ partial pressure for every cycle, as well as the adsorption capacity, calculated at the saturation point of the adsorbent. Note that, although the adsorption tests were repeated three times for each total pressure, the partial pressure in each test was obtained considering the experimental data of each test ($y_{H2O,in}$), as described through Equation 4.1; reason why its value is not constant throughout each total pressure.

$$p_{H_2O} = y_{H_2O,in} \times P_{total} \quad (4.1)$$

Table 4.1. Experimental results obtained for the adsorption experiments, at 250 ºC.

| $P_{total}$ / bar | $p_{H2O}$ / bar | $p_{H2O,average}$ / bar | $q_{H2O}$ / mol·g$^{-1}$ | $q_{H2O,average}$ / mol·g$^{-1}$ |
|---|---|---|---|---|
| 1 | 0.013 | 0.013±0.003 | 0.00147 | 0.00149±0.00006 |
| | 0.010 | | 0.00156 | |
| | 0.015 | | 0.00145 | |
| 4 | 0.055 | 0.060±0.006 | 0.00644 | 0.008±0.001 |
| | 0.066 | | 0.00847 | |
| | 0.060 | | 0.00774 | |
| 6 | 0.087 | 0.088±0.001 | 0.01332 | 0.012±0.001 |
| | 0.088 | | 0.01143 | |
| | 0.089 | | 0.01128 | |

Due to the uncertainty associated with the humidity transmitter, as well as the high sensitivity to temperature variations, the results presented for each pressure present slight variations, being, however, always in the same order of magnitude. For this reason, the average values obtained for each total pressure are also presented in Table 4.1.

Observing the results, it is noticeable that an increase in total pressure causes an increase in the adsorption capacity. This is due to a consequent increase in the number of gas molecules and more frequent collisions, which leads to higher probability of contact with the sorbent present in the column; in short, higher driving force for adsorption.

Although the literature on water adsorption capacity for zeolite 13X at this temperature and, especially, at such high pressures, is very scarce, it is worth mentioning that Mette *et al.* [62] achieved similar results for 0.010 bar of partial water pressure, obtaining for the adsorption capacity 0.00194 mol·g$^{-1}$ (representing, however, a deviation of 30 % as compared to the obtained value).

The experimental data was fitted against the Langmuir-Freundlich isotherm, expressed by Equation 4.2,

$$(q_{H_2O})_{LF} = \frac{q_{max,LF}\,(K_{LF}\,p_{H_2O})^{1/n}}{1 + (K_{LF}\,p_{H_2O})^{1/n}} \tag{4.2}$$

where $(q_{H_2O})_{LF}$ (mol·g$^{-1}$) represents the amount adsorbed estimated by the Langmuir-Freundlich isotherm, $q_{max,LF}$ (mol·g$^{-1}$) is the maximum adsorption capacity determined by the Langmuir-

Freundlich isotherm, $K_{LF}$ is the Langmuir-Freundlich adsorption constant ($bar^{-1}$) and n is a dimensionless parameter.

The fitting parameters of the Langmuir-Freundlich isotherm obtained for water adsorption are expressed in Table 4.2.

*Table 4.2. Fitted Langmuir-Freundlich parameters for water adsorption on zeolite 13X.*

| $q_{max,LF}$ / mol·g$^{-1}$ | $K_{LF}$ / bar$^{-1}$ | $1/n$ |
|---|---|---|
| 2.754 | 0.1047 | 1.160 |

The adsorption isotherm obtained experimentally, at 250 ºC, and through the model are presented in Figure 4.7. Although there is an apparent good adherence of the model, more experimental data should be gathered (only 4 experimental points for 3 fitting parameters).

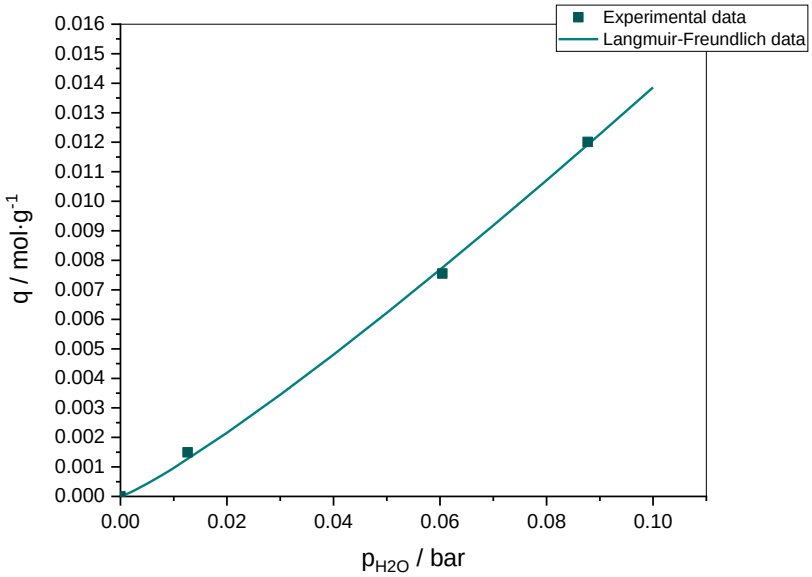



*Figure 4.7. Adsorption of $H_2O$ over zeolite 13X through experimental data (dots) and Langmuir-Freundlich predicted model (line), at 250 ºC.*

## 4.3 SER tests

The results obtained for the tests using the sorption-enhanced reactor are presented in Figure 4.8. The experiments were performed using a combination of $NiO/Al_2O_3$-$SiO_2$-CeO (methanation catalyst) and zeolite 13X (water adsorbent), on a mass ratio of 0.2:3.5 (so that the catalyst mass was the same used in both catalytic and SER tests), at 250 ºC and 1, 4 and 6 bar. Prior to the tests, the catalyst was activated at 650 ºC for 4 hours using a mixture of 10 mLn·min$^{-1}$ of $H_2$ and 90 mLn·min$^{-1}$ of $N_2$.

Figure 4.8 displays the results obtained by the infrared-based $CO_2$ and CO analyser, namely the molar fraction of $CO_2$ in the outlet stream and the evolution of $X_{CO2}$ with time. Also, the temperature profiles inside the reactor for both thermocouples are presented. The equilibrium conversion, previously obtained through Aspen Plus software (i.e., calculated based on pressure, temperature and feed composition), is also presented.

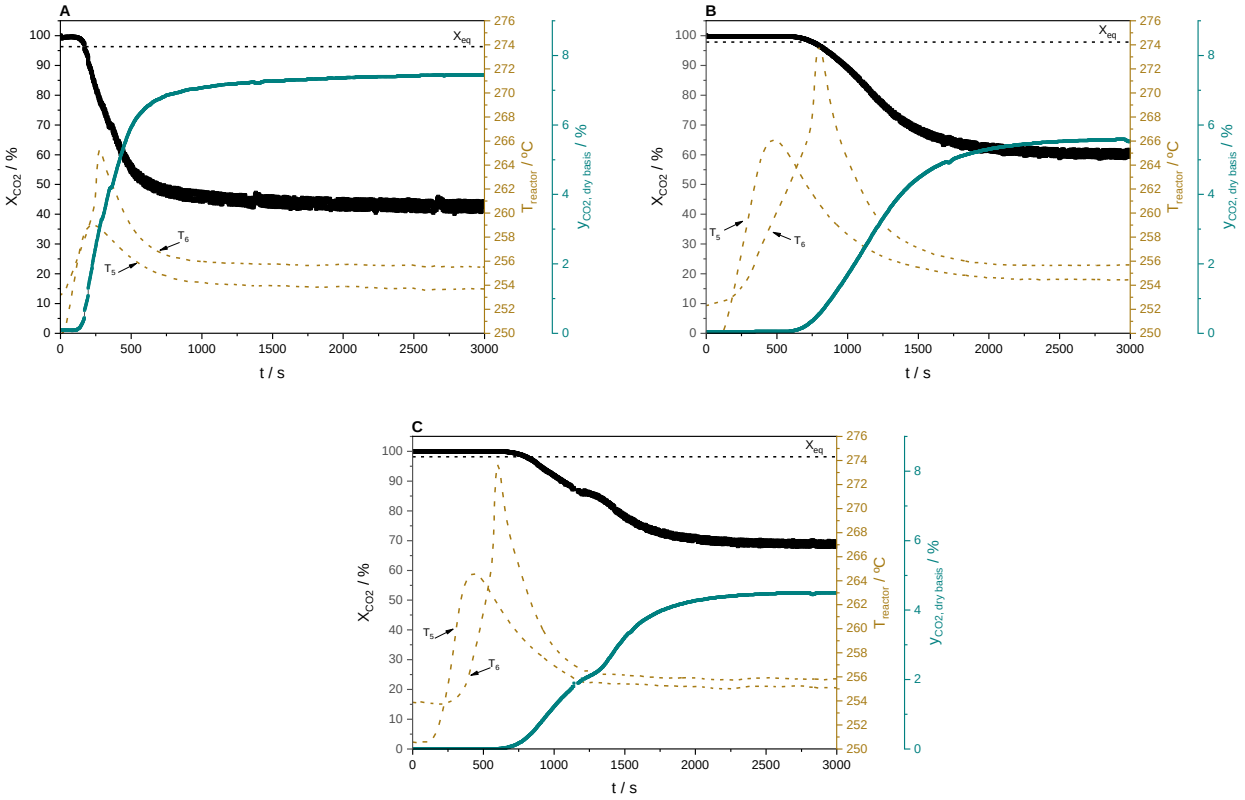



*Figure 4.8. SER performance at 250 ºC and 1 (A), 4 (B) and 6 (C) bar for $WHSV_{CO2}$ = 3 $Ln \cdot g^{-1} \cdot h^{-1}$ and $H_2/CO_2$ molar ratio = 4. The dotted black line represents the thermodynamic equilibrium calculated for the traditional reactor.*

From the analysis of Figure 4.8 it is possible to distinguish three distinct behaviours throughout the time of the sorption-enhanced methanation, for all pressures studied.

Firstly, during the pre-breakthrough stage, both methanation reaction and water adsorption occur, leading to total adsorption of the water produced during methanation by the zeolite and, consequently, favoring the direct methanation reaction and increasing the consumption of $CO_2$. Hence, in this first stage, total conversion of $CO_2$ is obtained, implying that the use of the SER allows overcoming not only the conversion obtained with a traditional reactor, but also the equilibrium one ($X_{eq}$). It is worth noting that the time of pre-breakthrough stage increases with pressure (1 bar – 109 s; 4 bar – 593 s; 6 bar – 636 s), as the adsorbent capacity also increases with this parameter; this is in accordance with the results obtained for the adsorption tests in the previous section. However, it must be considered that previous studies showed that the

presence of $CO_2$ during water adsorption on zeolites decreases their adsorption capacity by 15 % [9]. For this reason, a test using only zeolite was performed to assess if $CO_2$ adsorption occurred with zeolite 13X.

During this stage it is also observed that the reactor temperature shows a bigger increase when compared with the tests using the traditional reactor, being that, at 250 ºC and 4 bar, the average temperature increase of the SER was around 20 ºC, while for the traditional reactor it was around 8 ºC. This happens because in addition to the higher extent of the exothermic methanation reaction, water adsorption also occurs, and this phenomenon is also exothermic. Also, as both the Sabatier reaction and water adsorption are favored at higher pressures, the increase in temperature observed is higher for higher pressures.

In order to facilitate the understanding of the temperature profiles obtained for the SER, Figure 4.9 shows the temperature profiles obtained for a test using only catalyst and for an adsorption tests, performed at 250 ºC and 4 bar (intermediate pressure). As described in previous sections, the catalytic test was performed using a feed mixture of 10 mLn·min$^{-1}$ of $CO_2$, 40 mLn·min$^{-1}$ of $H_2$ and 50 mLn·min$^{-1}$ of $N_2$ and a $WHSV_{CO2}$ of 3 Ln·g$^{-1}$·h$^{-1}$, and the adsorption test was performed using 100 mLn·min$^{-1}$ of pure $N_2$ and 100 mLn·min$^{-1}$ of water-saturated $N_2$.

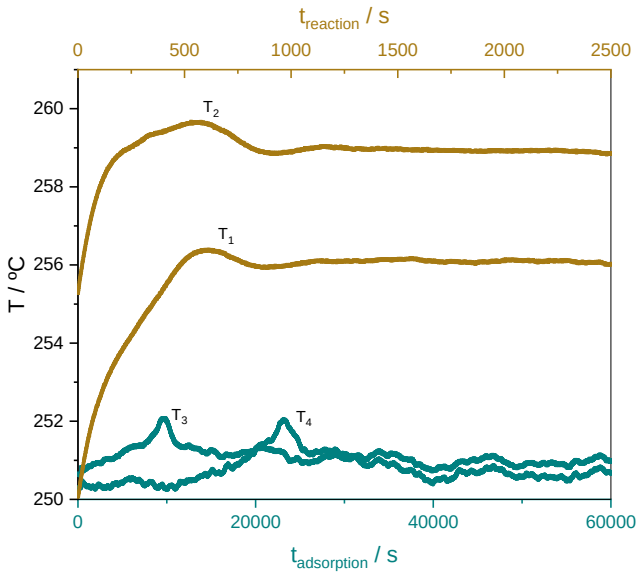



*Figure 4.9. Temperature profiles obtained inside the reactor/column for the catalytic ($T_1$ and $T_2$) and adsorption ($T_3$ and $T_4$) tests, respectively, at 250 ºC and 4 bar.*

From the figure above it is possible to observe that the adsorption process results in two temperature peaks that represent the passage of the adsorption wave through each of the column thermocouples ($T_3$ and $T_4$). These two peaks are also observed on the temperature profile of the sorption-enhanced reactor ($T_5$ and $T_6$), confirming the occurrence of adsorption. Again, as reaction is also occurring, the temperature increase is higher on the SER than the one on

either the methanation reaction or water adsorption alone at the same operating conditions. Although the temperature profiles for the other pressures are not shown, the results are similar, and so are the conclusions: the methanation reaction is the process that contributes the most for the temperature increase inside the reactor; however, the adsorption one occurs much faster in the SER than in the adsorption tests (as the amount of water produced during the reaction might be higher than the one considered in the adsorption tests), leading to a higher temperature increase than the one observed in Figure 4.9.

The second stage observed in Figure 4.8 corresponds to the breakthrough stage, during which a decrease in $X_{CO2}$ is observed, accompanied by an increase in the outlet mole fraction of $CO_2$. As the reaction carries on, water is continuously produced; however, the adsorbent eventually reaches the saturation point and the water adsorption decreases. As the adsorption process is inhibited, some $CO_2$ leaves the SER unconverted and a progressive decrease in temperature is also noticed (though, in part, this is also due to the heat loses through the reactor wall).

In the last stage, the post-breakthrough, the zeolite reaches its maximum adsorption capacity and adsorption no longer occurs. Hence, the reactor approximates the behaviour of a traditional one and all the parameters studied in Figure 4.8 tend to stabilize, i.e., steady state is reached.

For comparison reasons, the steady state $CO_2$ conversions obtained for the SER and the traditional reactor (TR), both obtained by chromatographic analysis, are presented in Table 4.3. To note that the results of $CO_2$ conversion obtained for the SER through chromatographic analysis are higher than the ones obtained using the infrared-based $CO_2$ and CO analyser.

*Table 4.3. $CO_2$ conversion obtained, at steady state, for the SER and the TR.*

| Pressure / bar | $X_{CO2,SER}$ / % | $X_{CO2,TR}$ / % |
|---|---|---|
| 1 | 49.2 | 62.6 |
| 4 | 65.2 | 72.5 |
| 6 | 71.9 | 76.9 |

Analysing the values presented in the table above, it is noticed a decrease in $CO_2$ conversion when the reaction was performed using the SER. Although this performance was not expected, it might be explained by experimental errors, namely the mass of catalyst used or the pressure, or even by the carbon balance error. However, at high pressures such deviations are within the overall uncertainity.

Considering the presented results, it was decided to study the effect of the presence of the zeolite, namely if zeolite 13X adsorbed any of the $CO_2$ present in the inlet and/or if it was able to catalyze any side reaction, causing $CO_2$ conversion to decrease.

Figure 4.10 shows the outlet flow rate of $CO_2$ during the breakthrough curve performed using the reactor filled with the same mixture of catalyst and zeolite, at 250 ºC and 4 bar (intermediate pressure under study). Prior to the experiment the reactor was heated to 300 ºC for 4 hours with a flow rate of 100 mLn·min$^{-1}$ of $N_2$ to ensure the zeolite was free of any compound.

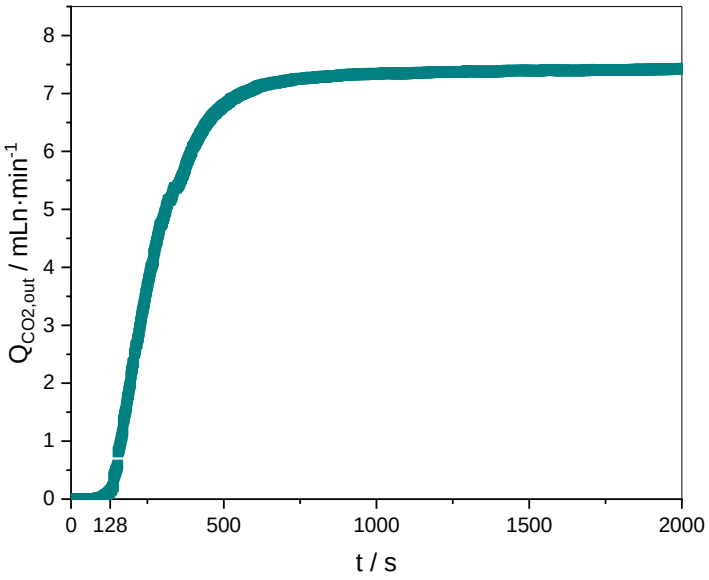



*Figure 4.10. $CO_2$ breakthrough curve for a feed composition of 7 mLn·min$^{-1}$ of $CO_2$ and 93 mLn·min$^{-1}$ of $N_2$, at 250 ºC and 4 bar.*

As can be observed from Figure 4.10, the analyser started detecting carbon dioxide on the outlet of the reactor after around 128 s, time after which the flow rate of $CO_2$ tends to the one injected in the feed. Since this time corresponds approximately to the delay in the set-up (130 s), determined by experiments performed using only inert, as explained in the previous chapter, it is possible to conclude that zeolite 13X does not adsorb any $CO_2$ at these experimental conditions, not influencing the performance of the SER.

Finally, a test using only zeolite as the reactor filling was performed to assess the catalytic activity of zeolite 13X under the conditions of the tests. The flow rate of $CO_2$ in the outlet stream during the test is presented in Figure 4.11.

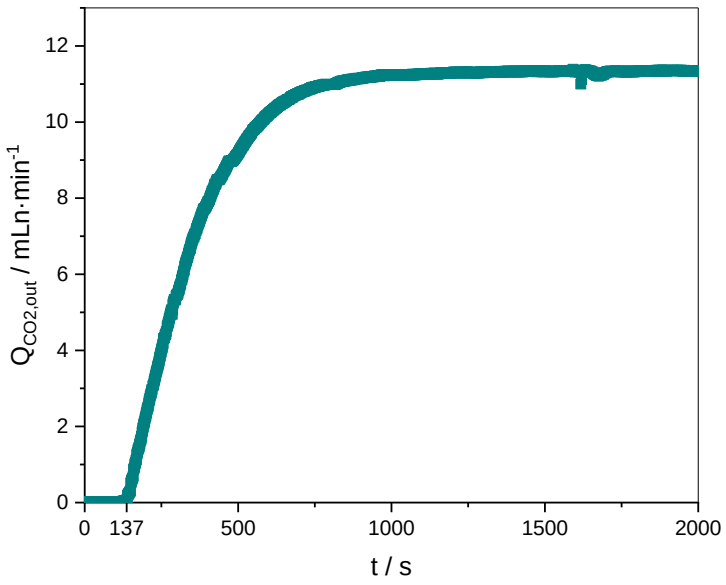



*Figure 4.11. $CO_2$ flow rate at the outlet for a feed composition of 10 mLn·min$^{-1}$ of $CO_2$, 40 mLn·min$^{-1}$ of $H_2$ and 50 mLn·min$^{-1}$ of $N_2$, at 250 ºC and 4 bar.*

From the results it is possible to observe that, after 137 s (delay in acquisition time) the analyser detects $CO_2$ and the flow rate stabilizes at around 11 mLn·min$^{-1}$. As this value is very close to the amount fed to the reactor (and the deviation can be justified by the uncertainty of the analysis equipment), it is possible to conclude that zeolite 13X does not present catalytic activity over the reactional mixture and no side reactions occur.

As a final remark, it is worth noting the performance achieved with the sorption-enhanced reactor (especially before the water breakthrough), as it allowed complete $CO_2$ conversion and the obtention of an almost pure methane stream (only small quantities of $H_2$ were detected), outperforming the traditional methanation reactor. Hence, having proven the effectiveness of using the SER, it can be expected that its use applied to biogas will allow the thermodynamic equilibrium conversion to be overcome and a biogas stream, almost completely consisting of methane, to be obtained.

However, and considering the possible scale-up of processes using this kind of multifunctional reactors, it should be taken into account that a continuous process is only achievable using more than one reactor. Figure 4.12 shows a schematic representation of a process running in two sorption-enhaced reactors, in parallel. It is possible to observe that, one of the SER is used to perform the reaction until the adsorbent saturation, while the other SER is being regenerated (usually by PSA or TSA). At the saturation point, the reactors switch functions, so that the process can run continuously.

One of the main issues of this multireactor process is the need to find regeneration conditions quickly enough to meet the saturation time of the adsorbent.

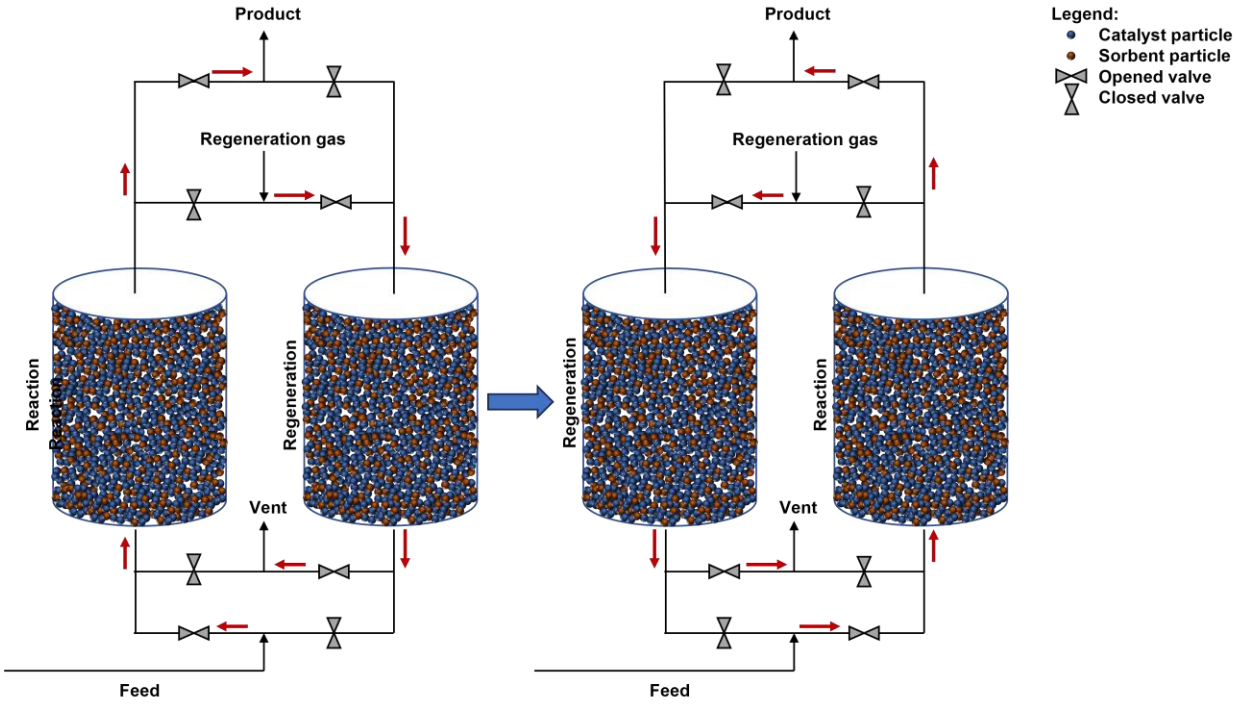



*Figure 4.12. Schematic representation of a process running in two sorption-enhanced-reactors.*

# 5 Conclusions

Prior to the proof of concept and evaluation of the SER performance, catalytic and adsorption tests were performed in order to study the influence of several parameters.

Firstly, a catalytic screening was performed in order to determine the best catalyst option to perform the parametric study. Having accomplished $CO_2$ conversions near 90 % for temperatures above 250 °C and 100 % $CH_4$ selectivity for all temperatures under study, and considering the greater availability, $NiO/Al_2O_3$-$SiO_2$-CeO was chosen to perform the remaining tests to evaluate the effect of reaction temperature, catalyst reduction temperature, gas velocity, pressure, and feed composition on $CO_2$ conversion.

Hence, an increase in $X_{CO2}$ was observed for higher temperatures and pressures (until 300 °C where a stabilization was observed), being that equilibrium conversion was almost attained at 300 (for 4 and 6 bar) and 350 °C (for 1, 4 and 6 bar), for $WHSV_{CO2}$=3 $Ln \cdot g^{-1} \cdot h^{-1}$. On the other hand, an increase in the reduction temperature (from 650 to 800 °C) produced negative effects, leading to lower catalytic performance. The study on gas velocity led to no significant differences, allowing to conclude that the reactional system was behaving without the influence of external mass transfer limitations. Also, the absence of $N_2$ in the feed produced no significant changes in either $CO_2$ conversion or temperature increase inside the reactor.

Water adsorption tests were performed using zeolite 13X at 250 °C. The influence of pressure was studied, allowing to conclude that an increase in pressure favors the water adsorption process, increasing the adsorption capacity. Also, the Langmuir-Freundlich equilibrium isotherm showed good adherence to the data, and the corresponding parameters were obtained.

Finally, both catalyst and zeolite mentioned above were integrated in the sorption-enhanced reactor to evaluate the benefits of using such multifunctional reactor on methane production. The SER was studied at 250 °C, temperature of interest considering the deviation of the obtained conversion from the equilibrium conversion, and at 1, 4 and 6 bar. The SER proved to be highly efficient for the Sabatier reaction, allowing to reach 100 % $CO_2$ conversion until the water breakthrough time for all pressures studied. Also, and due to an increase in adsorption capacity, an increase in pressure led to greater breakthrough times and, consequently, larger times in which the $CO_2$ conversion was complete.

Hence, considering the performance of the SER on the methanation process, it is possible to predict that its use in the process of biogas upgrading could bring great advantages regarding its efficiency.

# 6 Assessment of the work done

## 6.1 Objectives Achieved

The main goal of this work was to understand and study a SER on the enhancement of $CO_2$ methanation. For that, tests and characterizations of catalysts and an adsorbent were performed.

Regarding the tests performed with catalysts, the objectives were achieved, and the effect of several parameters on $CO_2$ conversion was studied.

The objectives defined for the adsorption tests were also fulfilled, having studied the adsorbent under three different pressures and analysing its adsorption capacity.

Finally, the main goal of the work was also achieved as the SER was proved to increase $CO_2$ conversion up to 100 %, during the period of time when it was able to perform as an adsorptive reactor (i.e., the adsorbent was not saturated), outperforming the traditional reactor and the equilibrium conversion defined based on feed conditions.

## 6.2 Final Assessment

The work carried out allowed me to get a closer insight of the investigation world, namely in the field of methanation and the use of multifunctional reactors for process enhancement. Also, it provided several challenges that led me to develop and deepen my critical thinking skills and autonomy.

Although all the goals of this work were met, there are some scenarios that would be interesting to study in future works.

Firstly, considering the biogas upgrading thematic, in which the SER is to be applied, an attractive scenario would be to evaluate its performance with a generic biogas feed, i.e., a feed containing $CO_2$ and $CH_4$, and check if the equilibrium shift still occurs, and to which extent. Still in this topic, different biogas composition could be studied, as well as the best operation conditions to perform biogas upgrading.

Also, in order to ensure the possibility of a continuous process, the best SER regeneration conditions (temperature and pressure) should be studied, so that the time needed for total regeneration meets the saturation time of the reactor.

# 7 References


[1] R. Wadanambi, L. Wandana, K. Chathumini, N. Dassanayake, D. Preethika, and U. Arachchige, "The effects of industrialization on climate change," *J. Res. Technol. Eng,* vol. 1, pp. 86-94, 2020.

[2] U. Nations. "Sustainable Development Goals." https://www.un.org/sustainabledevelopment/climate-change/ (accessed 22/02/2023, 2023).

[3] G. Rothenberg, "A realistic look at $CO_2$ emissions, climate change and the role of sustainable chemistry," *Sustainable Chemistry for Climate Action,* vol. 2, p. 100012, 2023, doi: 10.1016/j.scca.2023.100012.

[4] H. Ritchie, M. Roser, and P. Rosado, "$CO_2$ and greenhouse gas emissions," 2020.

[5] N. Mac Dowell, P. S. Fennell, N. Shah, and G. C. Maitland, "The role of $CO_2$ capture and utilization in mitigating climate change," *Nature Climate Change,* vol. 7, no. 4, pp. 243-249, 2017, doi: 10.1038/nclimate3231.

[6] A. Zachopoulos and E. Heracleous, "Overcoming the equilibrium barriers of $CO_2$ hydrogenation to methanol via water sorption: A thermodynamic analysis," *Journal of CO2 Utilization,* vol. 21, pp. 360-367, 2017, doi: 10.1016/j.jcou.2017.06.007.

[7] I. Agirre, E. Acha, J. F. Cambra, and V. L. Barrio, "Water sorption enhanced $CO_2$ methanation process: Optimization of reaction conditions and study of various sorbents," *Chemical Engineering Science,* vol. 237, p. 116546, 2021, doi: 10.1016/j.ces.2021.116546.

[8] A. Borgschulte, N. Gallandat, B. Probst, R. Suter, E. Callini, D. Ferri, Y. Arroyo, R. Erni, H. Geerlings, and A. Züttel, "Sorption enhanced $CO_2$ methanation," *Physical Chemistry Chemical Physics,* 10.1039/C3CP51408K vol. 15, no. 24, pp. 9620-9625, 2013, doi: 10.1039/C3CP51408K.

[9] S. Walspurger, G. D. Elzinga, J. W. Dijkstra, M. Sarić, and W. G. Haije, "Sorption enhanced methanation for substitute natural gas production: Experimental results and thermodynamic considerations," *Chemical Engineering Journal,* vol. 242, pp. 379-386, 2014, doi: 10.1016/j.cej.2013.12.045.

[10] A. I. Adnan, M. Y. Ong, S. Nomanbhay, K. W. Chew, and P. L. Show, "Technologies for biogas upgrading to biomethane: A review," *Bioengineering,* vol. 6, no. 4, p. 92, 2019, doi: 10.3390/bioengineering6040092.

[11] S. Fu, I. Angelidaki, and Y. Zhang, "In situ biogas upgrading by $CO_2$-to-$CH_4$ bioconversion," *Trends in Biotechnology,* vol. 39, no. 4, pp. 336-347, 2021, doi: 10.1016/j.tibtech.2020.08.006.

[12] D. Schmider, L. Maier, and O. Deutschmann, "Reaction kinetics of CO and $CO_2$ methanation over nickel," *Industrial & Engineering Chemistry Research,* vol. 60, no. 16, pp. 5792-5805, 2021, doi: 10.1021/acs.iecr.1c00389.

[13] T. Schaaf, J. Grünig, M. R. Schuster, T. Rothenfluh, and A. Orth, "Methanation of $CO_2$ - storage of renewable energy in a gas distribution system," *Energy, Sustainability and Society,* vol. 4, no. 1, p. 2, 2014, doi: 10.1186/s13705-014-0029-1.

[14] A. Sayyah, E. Mahmoudi, S. Farhoudi, G. Behmenyar, A. Z. Turan, S. R. Nabavi, and A. Niaei, "Environmental assessment of carbon dioxide methanation process using mixed metal oxide and zeolite-supported catalysts by life cycle assessment methodology," *Journal of Cleaner Production,* vol. 362, p. 132529, 2022, doi: 10.1016/j.jclepro.2022.132529.

[15] J. Ren, H. Lou, N. Xu, F. Zeng, G. Pei, and Z. Wang, "Methanation of CO/$CO_2$ for power to methane process: Fundamentals, status, and perspectives," *Journal of Energy Chemistry,* Article vol. 80, pp. 182-206, 2023, doi: 10.1016/j.jechem.2023.01.034.

[16] G. Jiajian, Q. Liu, F. Gu, B. Liu, Z. Zhong, and F. Su, "Recent advances in methanation catalysts for the production of synthetic natural gas," *RSC Adv.,* vol. 5, 2015, doi: 10.1039/C4RA16114A.

[17] Y. R. Dias and O. W. Perez-Lopez, "Carbon dioxide methanation over Ni-Cu/$SiO_2$ catalysts," *Energy Conversion and Management,* vol. 203, p. 112214, 2020, doi: 10.1016/j.enconman.2019.112214.

[18] J. Liu, C. Li, F. Wang, S. He, H. Chen, Y. Zhao, M. Wei, D. G. Evans, and X. Duan, "Enhanced low-temperature activity of $CO_2$ methanation over highly-dispersed Ni/$TiO_2$ catalyst," *Catalysis Science & Technology,* 10.1039/C3CY00355H vol. 3, no. 10, pp. 2627-2633, 2013, doi: 10.1039/C3CY00355H.

[19] S. Rönsch, J. Schneider, S. Matthischke, M. Schlüter, M. Götz, J. Lefebvre, P. Prabhakaran, and S. Bajohr, "Review on methanation - From fundamentals to current projects," (in english), *Fuel,* journal article vol. 166, pp. 276-296, 2016, doi: 10.1016/j.fuel.2015.10.111.

[20] P. Forzatti and L. Lietti, "Catalyst deactivation," *Catalysis Today,* vol. 52, no. 2, pp. 165-181, 1999, doi: 10.1016/S0920-5861(99)00074-7.

[21] M. Frey, D. Édouard, and A.-C. Roger, "Optimization of structured cellular foam-based catalysts for low-temperature carbon dioxide methanation in a platelet milli-reactor," *Comptes Rendus Chimie,* vol. 18, no. 3, pp. 283-292, 2015, doi: 10.1016/j.crci.2015.01.002.

[22] I. Ganesh, "Conversion of carbon dioxide into methanol – a potential liquid fuel: Fundamental challenges and opportunities (a review)," *Renewable and Sustainable Energy Reviews,* vol. 31, pp. 221-257, 2014, doi: 10.1016/j.rser.2013.11.045.

[23] C. H. Bartholomew, "Carbon deposition in steam reforming and methanation," *Catalysis Reviews-science and Engineering,* vol. 24, pp. 67-112, 1982, doi: 10.1080/03602458208079650.

[24] R. Delmelle, J. Terreni, A. Remhof, A. Heel, J. Proost, and A. Borgschulte, "Evolution of water diffusion in a sorption-enhanced methanation catalyst," *Catalysts,* vol. 8, no. 9, p. 341, 2018, doi: 10.3390/catal8090341.

[25] X. Gao, Z. Ge, G. Zhu, Z. Wang, J. Ashok, and S. Kawi, "Anti-coking and anti-sintering Ni/$Al_2O_3$ catalysts in the dry reforming of methane: Recent progress and prospects," *Catalysts,* vol. 11, no. 8, p. 1003, 2021, doi: 10.3390/catal11081003.

[26] X. Gao, J. Li, M. Zheng, S. Cai, J. Zhang, S. Askari, N. Dewangan, J. Ashok, and S. Kawi, "Recent progress in anti-coking Ni catalysts for thermo-catalytic conversion of greenhouse gases," *Process Safety and Environmental Protection,* vol. 156, pp. 598-616, 2021, doi: 10.1016/j.psep.2021.10.051.

[27] Y. Ramezani, F. Meshkani, and M. Rezaei, "Promotional effect of Mg in trimetallic nickel-manganese-magnesium nanocrystalline catalysts in $CO_2$ reforming of methane," *International Journal of Hydrogen Energy,* vol. 43, no. 49, pp. 22347-22356, 2018, doi: 10.1016/j.ijhydene.2018.09.222.

[28] B. Alrafei, I. Polaert, A. Ledoux, and F. Azzolina-Jury, "Remarkably stable and efficient Ni and Ni-Co catalysts for $CO_2$ methanation," *Catalysis Today,* vol. 346, pp. 23-33, 2020, doi: 10.1016/j.cattod.2019.03.026.

[29] H. Lu, X. Yang, G. Gao, J. Wang, C. Han, X. Liang, C. Li, Y. Li, W. Zhang, and X. Chen, "Metal (Fe, Co, Ce or La) doped nickel catalyst supported on $ZrO_2$ modified mesoporous

clays for CO and $CO_2$ methanation," *Fuel,* vol. 183, pp. 335-344, 2016, doi: 10.1016/j.fuel.2016.06.084.

[30] H. Muroyama, Y. Tsuda, T. Asakoshi, H. Masitah, T. Okanishi, T. Matsui, and K. Eguchi, "Carbon dioxide methanation over Ni catalysts supported on various metal oxides," *Journal of Catalysis,* vol. 343, pp. 178-184, 2016, doi: 10.1016/j.jcat.2016.07.018.

[31] A. C. Faria, R. Trujillano, V. Rives, C. V. Miguel, A. E. Rodrigues, and L. M. Madeira, "Cyclic operation of $CO_2$ capture and conversion into methane on Ni-hydrotalcite based dual function materials (DFMs)," *Journal of CO2 Utilization,* vol. 72, p. 102476, 2023, doi: 10.1016/j.jcou.2023.102476.

[32] A. Westermann, B. Azambre, M. C. Bacariza, I. Graça, M. F. Ribeiro, J. M. Lopes, and C. Henriques, "Insight into $CO_2$ methanation mechanism over NiUSY zeolites: An operando IR study," *Applied Catalysis B: Environmental,* vol. 174-175, pp. 120-125, 2015, doi: 10.1016/j.apcatb.2015.02.026.

[33] H. Fu, S. Sun, and H. Lian, "Enhanced low-temperature $CO_2$ methanation over Ni/ ZrO2-$Al_2O_3$ catalyst: Effect of Al addition on catalytic performance and reaction mechanism," *Journal of CO2 Utilization,* vol. 69, p. 102415, 2023, doi: 10.1016/j.jcou.2023.102415.

[34] T. A. Le, M. S. Kim, S. H. Lee, T. W. Kim, and E. D. Park, "CO and $CO_2$ methanation over supported Ni catalysts," *Catalysis Today,* vol. 293-294, pp. 89-96, 2017, doi: 10.1016/j.cattod.2016.12.036.

[35] Y. Artioli, "Adsorption," in *Encyclopedia of Ecology*, S. E. Jørgensen and B. D. Fath Eds. Oxford: Academic Press, 2008, pp. 60-65.

[36] D. D. Do, *Adsorption analysis: Equilibria and kinetics* (Series on Chemical Engineering, no. 2). World Scientific, 1998, p. 916.

[37] P. Webb, "Introduction to chemical adsorption analytical techniques and their applications to catalysis," 2003.

[38] P. HÚMpola, H. Odetti, A. Fertitta, and J. Vicente, "Thermodynamic analysis of adsorption models of phenol in liquid phase on different activated carbons," *Journal of the Chilean Chemical Society,* vol. 58, pp. 1541-1544, 2013, doi: 10.4067/S0717-97072013000100009.

[39] M. F. M. Post, "Chapter 11 Diffusion in zeolite molecular sieves," in *Studies in Surface Science and Catalysis*, vol. 58, H. van Bekkum, E. M. Flanigen, and J. C. Jansen Eds.: Elsevier, 1991, pp. 391-443.

[40] S. D. Faust and O. M. Aly, *Adsorption processes for water treatment*. Elsevier, 2013.

[41] A. Al Ezzi and H. Ma, "Equilibrium adsorption isotherm mechanism of water vapor on zeolites 3A, 4A, X, and Y," in *ASME 2017 International Mechanical Engineering Congress and Exposition*, 2017, vol. Volume 6: Energy, V006T08A059, doi: 10.1115/imece2017-72601.

[42] R. T. Yang, *Gas separation by adsorption processes*. World Scientific, 1997.

[43] A. M. Ribeiro, T. P. Sauer, C. A. Grande, R. F. P. M. Moreira, J. M. Loureiro, and A. E. Rodrigues, "Adsorption equilibrium and kinetics of water vapor on different adsorbents," *Industrial & Engineering Chemistry Research,* vol. 47, no. 18, pp. 7019-7026, 2008, doi: 10.1021/ie701732x.

[44] S. Weintraub, "Demystifying silica gel," *Object specialty group postprints,* vol. 9, pp. 169-194, 2002.

[45] R. Delmelle, R. B. Duarte, T. Franken, D. Burnat, L. Holzer, A. Borgschulte, and A. Heel, "Development of improved nickel catalysts for sorption enhanced $CO_2$ methanation," *International Journal of Hydrogen Energy,* vol. 41, no. 44, pp. 20185-20191, 2016, doi: 10.1016/j.ijhydene.2016.09.045.

[46] M. Ghodhbene, F. Bougie, P. Fongarland, and M. Iliuta, "Hydrophilic zeolite sorbents for in-situ water removal in high temperature processes," *The Canadian Journal of Chemical Engineering,* vol. 95, 2017, doi: 10.1002/cjce.22877.

[47] Z. Zhang, M. H. Ibrahim, M. H. El-Naas, and J. Cai, "Chapter 50 - Zeolites nanocomposite membrane applications in $CO_2$ capture," in *Handbook of Nanomaterials for Industrial Applications*, C. Mustansar Hussain Ed.: Elsevier, 2018, pp. 916-921.

[48] J. van Kampen, J. Boon, and M. van Sint Annaland, "Steam adsorption on molecular sieve 3A for sorption enhanced reaction processes," *Adsorption,* vol. 27, no. 4, pp. 577-589, 2021, doi: 10.1007/s10450-020-00283-8.

[49] A. Al-Ezzi and H. Ma, *Equilibrium Adsorption Isotherm Mechanism of Water Vapor on Zeolites 3A, 4A, X, and Y*. 2017, p. V006T08A059.

[50] M. Simo, S. Sivashanmugam, C. J. Brown, and V. Hlavacek, "Adsorption/desorption of water and ethanol on 3A zeolite in near-adiabatic fixed bed," *Industrial & Engineering Chemistry Research,* vol. 48, no. 20, pp. 9247-9260, 2009, doi: 10.1021/ie900446v.

[51] Y. Wang and M. D. LeVan, "Adsorption equilibrium of carbon dioxide and water vapor on zeolites 5A and 13X and silica gel: Pure components," *Journal of Chemical & Engineering Data,* vol. 54, no. 10, pp. 2839-2844, 2009, doi: 10.1021/je800900a.

[52] A. C. Dimian, C. S. Bildea, and A. A. Kiss, "Chapter 10 - Process intensification," in *Computer Aided Chemical Engineering*, vol. 35, A. C. Dimian, C. S. Bildea, and A. A. Kiss Eds.: Elsevier, 2014, pp. 397-448.

[53] R. Muthia, A. G. J. van der Ham, and A. A. Kiss, "Preliminary economic ranking of reactive distillation processes using a navigation method," in *Computer Aided Chemical Engineering*, vol. 43, A. Friedl, J. J. Klemeš, S. Radl, P. S. Varbanov, and T. Wallek Eds.: Elsevier, 2018, pp. 827-832.

[54] A. E. Rodrigues, Y.-j. Wu, L. M. Madeira, and R. Faria, *Sorption enhanced reaction processes*. World Scientific, 2017.

[55] K. Bizon, K. Skrzypek-Markiewicz, and M. Prończuk, "Numerical investigation of process enhancement using a bifunctional catalyst in a dual fluidized-bed reactor," *Catalysts,* vol. 11, no. 5, p. 530, 2021, doi: 10.3390/catal11050530.

[56] M. Grünewald and D. W. Agar, "Enhanced catalyst performance using integrated structured functionalities," *Chemical Engineering Science,* vol. 59, no. 22, pp. 5519-5526, 2004, doi: 10.1016/j.ces.2004.07.072.

[57] J. van Kampen, J. Boon, F. van Berkel, J. Vente, and M. van Sint Annaland, "Steam separation enhanced reactions: Review and outlook," *Chemical Engineering Journal,* vol. 374, pp. 1286-1303, 2019, doi: 10.1016/j.cej.2019.06.031.

[58] J. A. D. Dobladez, V. I. Á. Maté, S. Á. Torrellas, M. Larriba, G. Pascual Muñoz, and R. Alberola Sánchez, "Comparative simulation study of methanol production by $CO_2$ hydrogenation with 3A, 4A and 5A zeolites as adsorbents in a PSA reactor," *Separation and Purification Technology,* vol. 262, p. 118292, 2021, doi: 10.1016/j.seppur.2020.118292.

[59] A. Catarina Faria, C. V. Miguel, and L. M. Madeira, "Thermodynamic analysis of the $CO_2$ methanation reaction with in situ water removal for biogas upgrading," *Journal of CO2 Utilization,* vol. 26, pp. 271-280, 2018, doi: 10.1016/j.jcou.2018.05.005.

[60] M. A. Soria, C. Rocha, S. Tosti, A. Mendes, and L. M. Madeira, "$CO_x$ free hydrogen production through water-gas shift reaction in different hybrid multifunctional reactors," *Chemical Engineering Journal,* vol. 356, pp. 727-736, 2019, doi: 10.1016/j.cej.2018.09.044.

[61] Z. He, X. Wang, R. Liu, S. Gao, and T. Xiao, "Perfomances of different additives on NiO/γ-$Al_2O_3$ catalyst in CO methanation," *Applied Petrochemical Research,* vol. 6, no. 3, pp. 235-241, 2016, doi: 10.1007/s13203-016-0160-3.

[62] B. Mette, H. Kerskes, H. Drück, and H. Müller-Steinhagen, "Experimental and numerical investigations on the water vapor adsorption isotherms and kinetics of binderless zeolite 13X," *International Journal of Heat and Mass Transfer,* vol. 71, pp. 555-561, 2014, doi: 10.1016/j.ijheatmasstransfer.2013.12.061.